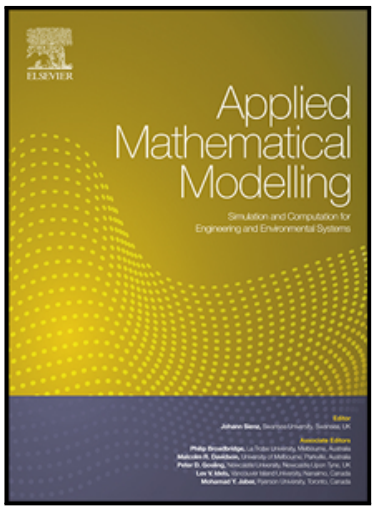

Chaos in fluid-conveying NSGT nanotubes with geometric imperfections

Mergen H. Ghayesh , Hamed Farokhi , Ali Farajpour

PII: S0307-904X(19)30269-0
DOI: https://doi.org/10.1016/j.apm.2019.04.053
Reference: APM 12800

To appear in: *Applied Mathematical Modelling*

Received date: 13 December 2018
Revised date: 11 April 2019
Accepted date: 30 April 2019

Please cite this article as: Mergen H. Ghayesh , Hamed Farokhi , Ali Farajpour , Chaos in fluid-conveying NSGT nanotubes with geometric imperfections, *Applied Mathematical Modelling* (2019), doi: https://doi.org/10.1016/j.apm.2019.04.053

Highlights

- Chaos in fluid-conveying nanotubes with initial deflections is analysed.
- A scale-dependent model of nanobeams with large deformations is developed.
- To comprehensively simulate size effects, the NSGT is utilised.
- Relative motions at the nanofluid/nanotube interface are incorporated.

Chaos in fluid-conveying NSGT nanotubes with geometric imperfections

Mergen H. Ghayesh [a], Hamed Farokhi [b], Ali Farajpour [a*]

[a] *School of Mechanical Engineering, University of Adelaide, South Australia 5005, Australia*

[b] *Department of Mechanical and Construction Engineering, Northumbria University, Newcastle upon Tyne NE1 8ST, UK*

[*] *Corresponding author's email: ali.farajpourouderji@adelaide.edu.au (A. Farajpour)*

Abstract

A scale-dependent model of nanobeams with large deformations is developed to investigate the influences of a geometric imperfection on the chaotic response of nanotubes. In order to comprehensively simulate the effects of being at nanoscales, a nonlocal strain gradient theory (NSGT) is utilised. To model a geometric imperfection, an initial deflection is taken into account for the nanosystem. Since the relative motion between the nanofluid and nanotube at the interface is not negligible, Karniadakis-Beskok assumptions are employed to incorporate the effects of this relative motion. Utilising an energy-work balance technique, the nonlinear governing equations are derived for the coupled motion of the nanofluid-conveying NSGT nanotube. Finally, the influences of the geometric imperfection on the motion response are analysed using a direct-time-integration approach and a Galerkin scheme.

Keywords: Chaotic response; Nanotubes; Nanofluid; Geometric imperfection

1. Introduction

The emergence of nanotechnology has brought promising solutions for many problems and challenges that human beings encounter. This relatively new branch of technology has many applications ranging from medicine to various engineering fields. Many useful nanotechnology-based systems such as nanoelectromechanical biosensors, energy harvesters and generators have been fabricated by researchers and engineers all around the world. Nanotubes are among the most common building blocks in these nanoscale systems. Therefore, it is important to improve our knowledge of the mechanical, physical and electrical behaviours of nanotubes.

Both experimental and theoretical investigations on small-scale structures have shown that their mechanical behaviour is size-dependent [1-6]. Size-dependent elasticity theories including surface [7-10], nonlocal [11-17], strain gradient [18-21] and couple stress [22-27] have been utilized in the literature for investigating the stability, oscillation and deformation of various types of nanostructures. In this nonlinear modelling, a combination of strain gradient and nonlocal theories is used [28-30].

The stability, oscillation and deformation of nanofluid-conveying nanotubes have been analysed in recent times via size-dependent elasticity theories. The vibration and instability of nanofluid-conveying nanotubes were theoretically explored by Wang and Ni [31] using an elasticity theory. Furthermore, a nanoscale system of a tube, surrounding matrix and fluid flow was analysed by Soltani et al. [32] in terms of mechanical response. In another analysis, Lee and Chang [33] investigated the time-dependent deformations of a fluid-conveying nanotube,

which vibrates in the thickness direction; they developed a nonlocal elasticity-based model for this problem. Moreover, a couple-stress elasticity-based model was introduced by Zeighampour and Beni [34] to analyse the influences of being at nanoscales as well as the effects of fluid-solid interactions on the vibrations of nanotubes. In another work reported in the literature, the effects of temperature changes and a viscoelastic foundation on the response of tubes conveying fluid at nanoscales were analysed [35]. Liang and Su [36] also developed a theoretical model to examine the stability of nanoscale tubes conveying a pulsating fluid. Furthermore, Maraghi et al. [37] utilised a nonlocal theory so as to analyse a nanoscale system of boron nitride nanotubes as well as fluid flow. A nonlocal theory was also applied by Oveissi et al. [38] to simulate size effects on the axial oscillations of nanofluid-conveying nanotubes. In addition to these investigations, continuum-based studies have been reported on the forced vibrations [39], wave dispersion [40] and nonlinear stability [41] of fluid-conveying nanotubes.

Perfectly straight nanotubes are rarely found in nanotechnology-based systems and devices since a small initial deflection is usually imposed on the nanotube during the fabrication process. It is important to incorporate the effects of this initial deflection as it has been indicated that a geometric imperfection affects the size-dependent mechanical response of small-scale structures [42, 43]. To the best of authors' knowledge, no continuum-based analysis has been conducted on the chaotic response of nanofluid-conveying nanotubes with a geometric imperfection. This encourages us to examine this problem in the current paper. The NSGT is employed to comprehensively model the effects of being at nanoscales. To take into consideration the effects of geometric imperfections, an initial deflection is assumed. The Karniadakis-Beskok assumptions are employed to simulate the effects of relative motion

between the nanofluid and nanotube at internal interface. The nonlinear governing equations are derived via an energy-work balance technique. Using a direct-time-integration approach and a Galerkin scheme, the size-dependent bifurcation characteristics of the system incorporating the effects of geometric imperfections are analysed and discussed.

2. Relative motion between nanofluid and nanotube at the interface

Let us consider homogeneous incompressible Newtonian fluid. In addition, the nanofluid flow is assumed to be fully developed and laminar. The pressure gradient is also considered constant through the tube. Furthermore, a constant viscosity as well as a constant density are taken into consideration for the nanofluid. A widely used hypothesis in macroscale structures conveying fluid is that there is no relative motion between fluid and structure at the interface. However, this hypothesis cannot be utilised in analysing nanoscale systems conveying fluid. To take into consideration the effects of this relative motion, let us define the Knudsen number (*Kn*) as follows

$$Kn = \frac{l_f}{l_e}. \tag{1}$$

Here l_f and l_e are respectively the average free path of molecules and external characteristic dimension. Using the Knudsen number, the viscosity is expressed as [44]

$$\mu_e = \frac{\mu_b}{\Lambda Kn + 1}, \tag{2}$$

where μ_b and μ_e, respectively, represent the bulk and effective viscosity. In Eq. (2), Λ is obtained by

$$\Lambda = \frac{2}{\pi}\Lambda_0 \tan^{-1}\left(\gamma_0 (Kn)^{\gamma_1}\right), \tag{3}$$

in which γ_0 and γ_1 are commonly assumed as $\gamma_0 = 4$ and $\gamma_1 = 0.4$, respectively. Moreover, Λ_0 is calculated as

$$\Lambda_0 = \lim_{Kn\to\infty} \Lambda = \frac{64\beta}{\left(-12\pi + 3\pi\beta\right)}. \tag{4}$$

Here β is a constant coefficient. A value of -1 is assumed for this coefficient. To take into consideration the effects of the relative motion between the nanofluid and nanotube at the interface, a speed correction factor (κ_c) is employed as

$$\kappa_c = \frac{U_{rm}}{U_{nrm}}, \tag{5}$$

where U_{rm} and U_{nrm} stand for the average nanofluid speed with and without relative motion at the interface, respectively. Using Navier–Stokes equations in conjunction with Eqs. (1)-(5) gives the following expression

$$\kappa_c = \left(Kn\Lambda + 1\right)\left\{\left(\frac{2}{\sigma_v} - 1\right)\left[\frac{4Kn}{\left(-Kn\beta + 1\right)}\right] + 1\right\}, \tag{6}$$

where σ_v indicates a constant associated with tangential momentum accommodations.

3. A nonlinear NSGT model incorporating geometric imperfections

A nanofluid-conveying NSGT nanotube with a geometric imperfection is indicated in Fig. 1. The length of the nanosystem is denoted by L. Furthermore, d_{out} and w_0 are employed to denote the outer diameter and initial deflection of the NSGT nanotube, respectively. The initial deflection is caused by geometric imperfections. In the fabrication process, due to many reasons such as the lack of precision in one stage of the process and uncontrolled initial thermal or mechanical stresses, geometric imperfections can be formed. The nonlinear longitudinal strain of the imperfect NSGT nanotube is

$$\varepsilon_{xx}=\frac{\partial w}{\partial x}\frac{dw_0}{dx}+\frac{1}{2}\left(\frac{\partial w}{\partial x}\right)^2+\frac{\partial u}{\partial x}-z\frac{\partial^2 w}{\partial x^2}. \tag{7}$$

In the above expression, w and u represent the transverse deflection and longitudinal displacement, respectively. The influences of shear deformations are not incorporated in the present formulation since the nanotube thickness is very small compared to its length in the analysis. For the same reason, the effects of thickness stretch are also neglected. Using the NSGT, the constitutive equation is written as

$$\left(1-\left(e_0\ell_c\right)^2\nabla^2\right)t_{xx}=t_{xx}^{cl}-\ell_{sg}^2\nabla^2 t_{xx}^{cl}=E\left(1-\ell_{sg}^2\nabla^2\right)\varepsilon_{xx}, \tag{8}$$

where t_{xx}^{cl}, t_{xx}, ℓ_{sg}, e_0, ℓ_c, ∇^2 and E indicate the classical stress, NSGT stress, strain gradient parameter, calibration constant, internal characteristic length, Laplace operator and Young's modulus, respectively [45-48]. In Eq. (8), $e_0\ell_c$ stands for the nonlocal parameter; the calibration constant (e_0) is calculated using experimental data or molecular dynamics; ℓ_c is an internal geometrical property of the nanosystem such as the bond length between two adjacent molecules. ℓ_{sg} is used to describe the strain gradient effect, which plays an important role at

ultrasmall levels. Indicating the cross-sectional area of the nanotube by *A*, the NSGT stress resultants are as

$$\left\langle N_{xx}, M_{xx} \right\rangle = \int_A \left\langle t_{xx}, z t_{xx} \right\rangle dA, \tag{9}$$

In the NSGT, there are two scale parameters, which make this theory reasonable for describing both strain gradient and nonlocal influences. Nonlocal influences play a significant role when the length of the structure is around several nanometres whereas strain gradient influences are important at higher lengths. Considering both of these influences leads to a suitable continuum model for nanoscale structures [28, 49, 50]. In view of Eqs. (7)-(9), the following relationships are obtained for the NSGT stress resultants

$$\left[1-\left(e_0 \ell_c\right)^2 \nabla^2\right] N_{xx} = \left(1-\ell_{sg}^2 \nabla^2\right) EA \left(\frac{\partial w}{\partial x}\frac{dw_0}{dx} + \frac{1}{2}\left(\frac{\partial w}{\partial x}\right)^2 + \frac{\partial u}{\partial x} \right), \tag{10}$$

$$\left[1-\left(e_0 \ell_c\right)^2 \nabla^2\right] M_{xx} = -\left(1-\ell_{sg}^2 \nabla^2\right) \left(EI \frac{\partial^2 w}{\partial x^2} \right), \tag{11}$$

in which *I* indicates the inertia moment of the tube. For convenience, the effects of size dependence in the thickness axis are not captured in the present analysis. Size-dependent theoretical models incorporating this effect have been recently proposed in the literature [51-53]. The effects of size dependence in the thickness axis on the mechanics of small-scale structures can be modelled in future analyses. The potential energy of the imperfect nanotube is written as

$$\begin{aligned} \delta U_{el} &= \int_0^L \int_A \left[\sigma_{xx}^{(1)} \nabla \delta\varepsilon_{xx} + \sigma_{xx} \delta\varepsilon_{xx} \right] dA dx = \left[\int_A \sigma_{xx}^{(1)} \delta\varepsilon_{xx} dA \right]_0^L \\ &+ \int_0^L \int_A \left[-\nabla \sigma_{xx}^{(1)} + \sigma_{xx} \right] \delta\varepsilon_{xx} dA dx, \end{aligned} \tag{12}$$

where $\sigma_{xx}^{(1)}$ and σ_{xx} stand for the first- and zeroth-order NSGT stresses, respectively. For the NSGT stresses of the imperfect nanotube, one obtains

$$t_{xx} = -\nabla\sigma_{xx}^{(1)} + \sigma_{xx}, \tag{13}$$

The motion energy of the imperfect nanofluid-conveying nanotube is also written as

$$\begin{aligned}\delta T_k = &\int_0^L \left(M\left(\frac{\partial u}{\partial t} + \kappa_c U\left(1 + \frac{\partial u}{\partial x} \right) \right)\left(\delta\frac{\partial u}{\partial t} + \kappa_c U\delta\frac{\partial u}{\partial x} \right) + m\frac{\partial u}{\partial t}\delta\frac{\partial u}{\partial t} \right) dx \\ &+ \int_0^L \left(M\left(\frac{\partial w}{\partial t} + \kappa_c U\left(\frac{\partial w}{\partial x} + \frac{dw_0}{dx} \right) \right)\left(\delta\frac{\partial w}{\partial t} + \kappa_c U\delta\frac{\partial w}{\partial x} \right) + m\frac{\partial w}{\partial t}\delta\frac{\partial w}{\partial t} \right) dx.\end{aligned} \tag{14}$$

In Eq. (14), *M, m* and *U* represent the nanofluid mass per length, the tube mass per length and the nanofluid speed, respectively. Moreover, the work (W_F) due to the external force (i.e. $F(x)\cos(\omega t)$) is given by

$$\delta W_F = \int_0^L \left[F(x)\cos(\omega t) \right]\delta w \, dx. \tag{15}$$

It should be noticed that ω is the excitation frequency while *F* is the excitation amplitude. The energy-work balance technique can be written as

$$\int_{t_1}^{t_2} \left[-\delta U_{el} + \delta W_F + \delta T_k \right] dt = 0. \tag{16}$$

The substitution of Eqs. (12), (14) and (15) into Eq. (16) gives

$$\frac{\partial N_{xx}}{\partial x} = MU^2\kappa_c^2\frac{\partial^2 u}{\partial x^2} + (m+M)\frac{\partial^2 u}{\partial t^2} + 2MU\kappa_c\frac{\partial^2 u}{\partial x \partial t}, \tag{17}$$

$$\begin{aligned}&\frac{\partial^2 M_{xx}}{\partial x^2} + \frac{\partial}{\partial x}\left(N_{xx}\left(\frac{dw_0}{dx} + \frac{\partial w}{\partial x} \right) \right) + \cos(\omega t)F(x) = \\ &MU^2\kappa_c^2\left(\frac{d^2 w_0}{dx^2} + \frac{\partial^2 w}{\partial x^2} \right) + (m+M)\frac{\partial^2 w}{\partial t^2} + 2MU\kappa_c\frac{\partial^2 w}{\partial t \partial x}.\end{aligned} \tag{18}$$

Applying Eqs. (17) and (18) in conjunction with Eqs. (10) and (11), the following expressions are derived for the NSGT stress resultants

$$N_{xx}=EA\left(1-\ell_{sg}^{2}\nabla^{2}\right)\left(\frac{dw_{0}}{dx}\frac{\partial w}{\partial x}+\frac{1}{2}\left(\frac{\partial w}{\partial x}\right)^{2}+\frac{\partial u}{\partial x}\right)$$
$$+\left(e_{0}\ell_{c}\right)^{2}\left(MU^{2}\kappa_{c}^{2}\frac{\partial^{3}u}{\partial x^{3}}+\left(m+M\right)\frac{\partial^{3}u}{\partial x\partial t^{2}}+2MU\kappa_{c}\frac{\partial^{3}u}{\partial t\partial x^{2}}\right), \tag{19}$$

$$M_{xx}=-\left(1-\ell_{sg}^{2}\nabla^{2}\right)\left(EI\frac{\partial^{2}w}{\partial x^{2}}\right)+\left(e_{0}\ell_{c}\right)^{2}\left(m+M\right)\frac{\partial^{2}w}{\partial t^{2}}$$
$$-\left(e_{0}\ell_{c}\right)^{2}\frac{\partial}{\partial x}\left(N_{xx}\left(\frac{dw_{0}}{dx}+\frac{\partial w}{\partial x}\right)\right)-\left(e_{0}\ell_{c}\right)^{2}\cos\left(\omega t\right)F\left(x\right) \tag{20}$$
$$+\left(e_{0}\ell_{c}\right)^{2}\left[MU^{2}\kappa_{c}^{2}\left(\frac{d^{2}w_{0}}{dx^{2}}+\frac{\partial^{2}w}{\partial x^{2}}\right)+2MU\kappa_{c}\frac{\partial^{2}w}{\partial t\partial x}\right].$$

Utilising Eqs. (17)-(20), and then employing the following dimensionless parameters

$$\left\langle w^{*},u^{*},w_{0}^{*}\right\rangle=\frac{1}{d_{out}}\left\langle w,u,w_{0}\right\rangle,\quad\left\langle x^{*},\eta_{nl},\eta_{sg}\right\rangle=\frac{1}{L}\left\langle x,e_{0}\ell_{c},\ell_{sg}\right\rangle,$$
$$\Pi=\frac{AL^{2}}{I},\quad t^{*}=\frac{t}{L^{2}}\left[\frac{EI}{\left(M+m\right)}\right]^{\frac{1}{2}},\quad\alpha=\frac{L}{d_{out}},\quad\Upsilon=\frac{M}{m+M}, \tag{21}$$
$$\omega^{*}=L^{2}\left[\frac{\left(M+m\right)}{EI}\right]^{\frac{1}{2}}\omega,\ U^{*}=L\left(\frac{M}{EI}\right)^{\frac{1}{2}}U,\ F^{*}=\frac{L^{4}F}{d_{out}EI},\ \bar{\nabla}^{2}=\frac{\partial^{2}}{\partial x^{*2}},$$

the non-dimensional nonlinear differential equations of the nanofluid-conveying NSGT nanotube are derived as

$$
\begin{aligned}
&\frac{\alpha}{\Pi}\left(\frac{\partial^2 u}{\partial t^2}+2\kappa_c\sqrt{\Upsilon}U\frac{\partial^2 u}{\partial x\partial t}+\kappa_c^2U^2\frac{\partial^2 u}{\partial x^2}\right)\\
&-\frac{\alpha}{\Pi}\eta_{nl}^2\left(\frac{\partial^4 u}{\partial x^2\partial t^2}+2\kappa_c\sqrt{\Upsilon}U\frac{\partial^4 u}{\partial t\partial x^3}+\kappa_c^2U^2\frac{\partial^4 u}{\partial x^4}\right)\\
&-\frac{\partial}{\partial x}\left(\frac{dw_0}{dx}\frac{\partial w}{\partial x}+\frac{1}{2}\left(\frac{\partial w}{\partial x}\right)^2+\alpha\frac{\partial u}{\partial x}\right)\\
&+\eta_{sg}^2\frac{\partial^3}{\partial x^3}\left(\frac{dw_0}{dx}\frac{\partial w}{\partial x}+\frac{1}{2}\left(\frac{\partial w}{\partial x}\right)^2+\alpha\frac{\partial u}{\partial x}\right)=0,
\end{aligned}
\tag{22}
$$

$$
\begin{aligned}
&\frac{\partial^2 w}{\partial t^2}+\kappa_c^2U^2\left(\frac{d^2w_0}{dx^2}+\frac{\partial^2 w}{\partial x^2}\right)+2\kappa_c\sqrt{\Upsilon}U\frac{\partial^2 w}{\partial t\partial x}\\
&-\eta_{nl}^2\left(\frac{\partial^4 w}{\partial x^2\partial t^2}+2\kappa_c\sqrt{\Upsilon}U\frac{\partial^4 w}{\partial t\partial x^3}+\kappa_c^2U^2\left(\frac{\partial^4 w}{\partial x^4}+\frac{d^4w_0}{dx^4}\right)\right)\\
&-F_1\cos(\omega t)-\eta_{sg}^2\frac{\partial^6 w}{\partial x^6}+\frac{\partial^4 w}{\partial x^4}\\
&-\frac{\Pi}{\alpha^2}\frac{\partial}{\partial x}\left\{\left(\frac{dw_0}{dx}+\frac{\partial w}{\partial x}\right)\left[\frac{dw_0}{dx}\frac{\partial w}{\partial x}+\frac{1}{2}\left(\frac{\partial w}{\partial x}\right)^2+\alpha\frac{\partial u}{\partial x}\right]\right.\\
&-\eta_{sg}^2\left(\frac{dw_0}{dx}+\frac{\partial w}{\partial x}\right)\frac{\partial^2}{\partial x^2}\left[\frac{dw_0}{dx}\frac{\partial w}{\partial x}+\frac{1}{2}\left(\frac{\partial w}{\partial x}\right)^2+\alpha\frac{\partial u}{\partial x}\right]\\
&\left.+\frac{\alpha}{\Pi}\eta_{nl}^2\left(\frac{dw_0}{dx}+\frac{\partial w}{\partial x}\right)\left[\frac{\partial^3 u}{\partial x\partial t^2}+2\kappa_c\sqrt{\Upsilon}U\frac{\partial^3 u}{\partial t\partial x^2}+\kappa_c^2U^2\frac{\partial^3 u}{\partial x^3}\right]\right\}\\
&+\frac{\Pi}{\alpha^2}\eta_{nl}^2\frac{\partial^3}{\partial x^3}\left\{\left(\frac{\partial w}{\partial x}+\frac{dw_0}{dx}\right)\left[\frac{dw_0}{dx}\frac{\partial w}{\partial x}+\frac{1}{2}\left(\frac{\partial w}{\partial x}\right)^2+\alpha\frac{\partial u}{\partial x}\right]\right.\\
&-\eta_{sg}^2\left(\frac{\partial w}{\partial x}+\frac{dw_0}{dx}\right)\frac{\partial^2}{\partial x^2}\left[\frac{dw_0}{dx}\frac{\partial w}{\partial x}+\frac{1}{2}\left(\frac{\partial w}{\partial x}\right)^2+\alpha\frac{\partial u}{\partial x}\right]\\
&\left.+\frac{\alpha}{\Pi}\eta_{nl}^2\left(\frac{\partial w}{\partial x}+\frac{dw_0}{dx}\right)\left(\frac{\partial^3 u}{\partial x\partial t^2}+2\kappa_c\sqrt{\Upsilon}U\frac{\partial^3 u}{\partial t\partial x^2}+\kappa_c^2U^2\frac{\partial^3 u}{\partial x^3}\right)\right\}=0.
\end{aligned}
\tag{23}
$$

It should be noticed that for simplification purposes, asterisk notations are not considered. When the fluid velocity and fluid mass are set to zero, the governing equations (i.e. Eqs. (22) and (23)) are reduced to those available in the literature for Euler-Bernoulli nanobeams without

axial inertia effects [54-57]. Let us assume an imperfect NSGT nanotube with clamped ends. The displacements of the nanotube are given by

$$\begin{Bmatrix} u \\ w \end{Bmatrix} = \begin{Bmatrix} \sum_{k=1}^{N_x} \phi_k^{(u)}(x) r_k(t) \\ \sum_{k=1}^{N_z} \phi_k^{(w)}(x) q_k(t) \end{Bmatrix}, \tag{24}$$

where $\varphi_k^{(w)}$ and $\phi_k^{(u)}$ denote transverse and longitudinal trial functions, respectively; r_k and q_k, respectively, denote transverse and longitudinal generalised coordinates [58-60]. Indicating the imperfection amplitude by A_0, one can write the initial defection as $w_0 = A_0\phi_1^{(w)}$. Substituting Eq. (24) into Eqs. (22) and (23) gives

$$\begin{aligned}
&\frac{\alpha}{\Pi}\int_0^1 \Bigg(\sum_{k=1}^{N_x} \frac{d^2 r_k}{dt^2}\phi_i^{(u)}\phi_k^{(u)} + 2\kappa_c\sqrt{\Upsilon}U\sum_{k=1}^{N_x}\frac{dr_k}{dt}\phi_i^{(u)}\frac{d\phi_k^{(u)}}{dx} \\
&+\kappa_c^2 U^2 \sum_{k=1}^{N_x} r_k \phi_i^{(u)} \frac{d^2\phi_k^{(u)}}{dx^2}\Bigg)dx - \frac{\alpha}{\Pi}\eta_{nl}^2\int_0^1 \Bigg[\sum_{k=1}^{N_x}\frac{d^2 r_k}{dt^2}\phi_i^{(u)}\frac{d^2\phi_k^{(u)}}{dx^2} \\
&+2\kappa_c\sqrt{\Upsilon}U\sum_{k=1}^{N_x}\frac{dr_k}{dt}\phi_i^{(u)}\frac{d^3\phi_k^{(u)}}{dx^3} + \kappa_c^2U^2\sum_{k=1}^{N_x} r_k\phi_i^{(u)}\frac{d^4\phi_k^{(u)}}{dx^4}\Bigg]dx \\
&-\int_0^1 \phi_i^{(u)}\frac{d}{dx}\Bigg(\alpha\sum_{k=1}^{N_x} r_k\frac{d\phi_k^{(u)}}{dx} + \frac{1}{2}\sum_{j=1}^{N_z}\sum_{k=1}^{N_z} q_j q_k \frac{d\phi_j^{(w)}}{dx}\frac{d\phi_k^{(w)}}{dx} \\
&+A_0\sum_{k=1}^{N_z} q_k\frac{d\phi_k^{(w)}}{dx}\frac{d\phi_1^{(w)}}{dx}\Bigg)dx + \eta_{sg}^2\int_0^1 \phi_i^{(u)}\frac{d^3}{dx^3}\Bigg(\alpha\sum_{k=1}^{N_x}\frac{d\phi_k^{(u)}}{dx}r_k \\
&+\frac{1}{2}\sum_{j=1}^{N_z}\sum_{k=1}^{N_z}\frac{d\phi_j^{(w)}}{dx}\frac{d\phi_k^{(w)}}{dx}q_j q_k + A_0\sum_{k=1}^{N_z}\frac{d\phi_k^{(w)}}{dx}\frac{d\phi_1^{(w)}}{dx}q_k\Bigg)dx = 0,
\end{aligned} \tag{25}$$

$$\int_0^1 \left\{ \sum_{k=1}^{N_z} \frac{d^2 q_k}{dt^2} \phi_i^{(w)} \phi_k^{(w)} + 2\kappa_c \sqrt{\Upsilon} U \sum_{k=1}^{N_z} \frac{dq_k}{dt} \phi_i^{(w)} \frac{d\phi_k^{(w)}}{dx} \right.$$

$$\left. + \kappa_c^2 U^2 \left[\sum_{k=1}^{N_z} q_k \phi_i^{(w)} \frac{d^2 \phi_k^{(w)}}{dx^2} + A_0 \phi_i^{(w)} \frac{d^2 \phi_1^{(w)}}{dx^2} \right] \right\} dx$$

$$- \eta_{nl}^2 \int_0^1 \left\{ \sum_{k=1}^{N_z} \frac{d^2 q_k}{dt^2} \phi_i^{(w)} \frac{d^2 \phi_k^{(w)}}{dx^2} + 2\kappa_c \sqrt{\Upsilon} U \sum_{k=1}^{N_z} \frac{dq_k}{dt} \phi_i^{(w)} \frac{d^3 \phi_k^{(w)}}{dx^3} \right.$$

$$\left. + \kappa_c^2 U^2 \left[\sum_{k=1}^{N_z} q_k \phi_i^{(w)} \frac{d^4 \phi_k^{(w)}}{dx^4} + A_0 \phi_i^{(w)} \frac{d^4 \phi_1^{(w)}}{dx^4} \right] \right\} dx - F_1 \int_0^1 \phi_i^{(w)} \cos(\omega t) dx$$

$$+ \int_0^1 \left(-\eta_{sg}^2 \sum_{k=1}^{N_z} q_k \phi_i^{(w)} \frac{d^6 \phi_k^{(w)}}{dx^6} + \sum_{k=1}^{N_z} q_k \phi_i^{(w)} \frac{d^4 \phi_k^{(w)}}{dx^4} \right) dx$$

$$- \frac{\Pi}{\alpha^2} \int_0^1 \left(\phi_i^{(w)} \frac{d}{dx} \left\{ \left(A_0 \frac{d\phi_1^{(w)}}{dx} + \sum_{k=1}^{N_z} q_k \frac{d\phi_k^{(w)}}{dx} \right) \left(\alpha \sum_{k=1}^{N_x} r_k \frac{d\phi_k^{(u)}}{dx} \right.\right.\right.$$

$$\left. + A_0 \sum_{k=1}^{N_z} q_k \frac{d\phi_k^{(w)}}{dx} \frac{d\phi_1^{(w)}}{dx} + \frac{1}{2} \sum_{j=1}^{N_z} \sum_{k=1}^{N_z} q_j q_k \frac{d\phi_j^{(w)}}{dx} \frac{d\phi_k^{(w)}}{dx} \right)$$

$$- \eta_{sg}^2 \left(A_0 \frac{d\phi_1^{(w)}}{dx} + \sum_{k=1}^{N_z} q_k \frac{d\phi_k^{(w)}}{dx} \right) \frac{d^2}{dx^2} \left(\alpha \sum_{k=1}^{N_x} r_k \frac{d\phi_k^{(u)}}{dx} \right.$$

$$\left. + A_0 \sum_{k=1}^{N_z} q_k \frac{d\phi_k^{(w)}}{dx} \frac{d\phi_1^{(w)}}{dx} + \frac{1}{2} \sum_{j=1}^{N_z} \sum_{k=1}^{N_z} q_j q_k \frac{d\phi_j^{(w)}}{dx} \frac{d\phi_k^{(w)}}{dx} \right)$$

$$+ \frac{\alpha}{\Pi} \eta_{nl}^2 \left(\sum_{k=1}^{N_z} q_k \frac{d\phi_k^{(w)}}{dx} + A_0 \frac{d\phi_1^{(w)}}{dx} \right) \left(\sum_{k=1}^{N_x} \frac{d^2 r_k}{dt^2} \frac{d\phi_k^{(u)}}{dx} \right.$$

$$\left.\left.\left. + 2\kappa_c \sqrt{\Upsilon} U \sum_{k=1}^{N_x} \frac{dr_k}{dt} \frac{d^2 \phi_k^{(u)}}{dx^2} + \kappa_c^2 U^2 \sum_{k=1}^{N_x} r_k \frac{d^3 \phi_k^{(u)}}{dx^3} \right) \right\} \right) dx$$

$$+ \frac{\Pi}{\alpha^2} \eta_{nl}^2 \int_0^1 \left(\phi_i^{(w)} \frac{d^3}{dx^3} \left\{ \left(A_0 \frac{d\phi_1^{(w)}}{dx} + \sum_{k=1}^{N_z} q_k \frac{d\phi_k^{(w)}}{dx} \right) \left(\alpha \sum_{k=1}^{N_x} r_k \frac{d\phi_k^{(u)}}{dx} \right.\right.\right.$$

$$\left. + A_0 \sum_{k=1}^{N_z} q_k \frac{d\phi_k^{(w)}}{dx} \frac{d\phi_1^{(w)}}{dx} + \frac{1}{2} \sum_{j=1}^{N_z} \sum_{k=1}^{N_z} q_j q_k \frac{d\phi_j^{(w)}}{dx} \frac{d\phi_k^{(w)}}{dx} \right)$$

$$
\begin{aligned}
&-\eta_{sg}^2\left(A_0\frac{d\phi_1^{(w)}}{dx}+\sum_{k=1}^{N_z}q_k\frac{d\phi_k^{(w)}}{dx}\right)\frac{d^2}{dx^2}\left(\alpha\sum_{k=1}^{N_x}r_k\frac{d\phi_k^{(u)}}{dx}\right.\\
&\left.+A_0\sum_{k=1}^{N_z}q_k\frac{d\phi_k^{(w)}}{dx}\frac{d\phi_1^{(w)}}{dx}+\frac{1}{2}\sum_{j=1}^{N_z}\sum_{k=1}^{N_z}q_jq_k\frac{d\phi_j^{(w)}}{dx}\frac{d\phi_k^{(w)}}{dx}\right)\\
&+\frac{\alpha}{\Pi}\eta_{nl}^2\left(A_0\frac{d\phi_1^{(w)}}{dx}+\sum_{k=1}^{N_z}q_k\frac{d\phi_k^{(w)}}{dx}\right)\left(\sum_{k=1}^{N_x}\frac{d^2r_k}{dt^2}\frac{d\phi_k^{(u)}}{dx}\right.\\
&\left.\left.+2\kappa_c\sqrt{\Upsilon}U\sum_{k=1}^{N_x}\frac{dr_k}{dt}\frac{d^2\phi_k^{(u)}}{dx^2}+\kappa_c^2U^2\sum_{k=1}^{N_x}r_k\frac{d^3\phi_k^{(u)}}{dx^3}\right)\right\}\right)dx=0.
\end{aligned}
\tag{26}
$$

The above set of time-dependent coupled equations is solved via application of a direct-time-integration technique.

4. Numerical results

The chaotic response of a NSGT nanotube with a geometric imperfection is analysed in the following section. For the NSGT nanotube, we have E=610 MPa, v=0.3, density=1024 kg/m^3, h=66.0 nm, R_{out} =290.5 nm and L/d_{out} =20. Moreover, the dimensionless parameters are κ_c =1.10, Υ =0.5915, Π = 4006.9411, α =20.0, $\eta_{sg}=0.04$ and $\eta_{nl}=0.10$. In the solution procedure, a dimensionless damping coefficient of 0.1 is assumed for both u and w motions. Ten degrees of freedom are chosen in each direction. The non-dimensional imperfection amplitude is defined by dividing this parameter by the thickness. In the current nonlinear analysis, the excitation frequency is equal to the first transverse natural frequency.

To demonstrate the accuracy of the size-dependent modelling, the dimensionless linear critical velocities are compared with those calculated in Refs. [61, 62]; the comparison is shown in Fig. 2. The dimensionless critical velocity and nonlocal parameter are defined as

$U^* = U\sqrt{ML^2/EI}$ and $\eta_{nl} = e_0\ell_c/L$, respectively. Slip influences and the effects of applied load as well as strain gradient effects are ignored. Figure 2 indicates a very good agreement between the calculated results and those reported in Refs. [61, 62].

The convergence of the presented numerical solution is investigated in Fig. 3 for A_0=0.01 and U = 5.00. The bifurcation of fluid-conveying NSGT tubes is plotted for 4-DOF, 8-DOF, 16-DOF and 20-DOF. From this figure, it is seen that the number of DOF plays an important role in the bifurcation behaviour. While taking into account 4 DOF does not lead to a converged solution, in the case of 20-DOF, the numerical solution is converged.

The bifurcation of fluid-conveying NSGT tubes for the size-dependent dynamics along both x and z directions is plotted in Fig. 4; the amplitude of initial deflection, nanofluid speed and natural frequency are A_0=0, U = 4.90 and ω_1=2.1837, respectively. It is found that at small forcing amplitudes, the motion is of a periodic type. Nonetheless, as the forcing amplitude is increased, a highly chaotic behaviour is observed for the NSGT nanotube without initial deflection. This is owing to the fact that higher transverse loads cause more chaos in the mechanical behaviour of the tube at nanoscales.

Figure 5 shows the bifurcation of fluid-conveying NSGT tubes for the size-dependent dynamics along both x and z directions; in this figure, the imperfection amplitude is set to A_0=0.005 whereas the nanofluid speed is the same as the previous figure (i.e. U = 4.90). The natural frequency is ω_1=4.9808. Again, at small forcing amplitudes, the size-dependent motion is of a periodic type. Nevertheless, various motion types involving period-2, period-4 and quasiperiodic are observed when the forcing amplitude is increased. Comparing Figs. 4 and 5

reveals that implementing a small initial deflection can considerably reduce chaotic response of the nanofluid-conveying NSGT nanotube. This is because of the fact that implementing a small initial deflection can slightly make the nanosystem stronger and more stable. Figures 6 and 7 are plotted so as to provide the reader with more data about the size-dependent dynamics of the NSGT nanotube of Fig. 5. It is concluded that at F_1=11.0, the system undergoes a period-2 motion whereas it encounters a quasiperiodic response at F_1=37.8.

The size-dependent bifurcation of fluid-conveying NSGT tubes for dynamic responses along both *x* and *z* directions is shown in Fig. 8; the amplitude of initial deflection, nanofluid speed and natural frequency are set to A_0=0.01, U=4.90 and ω_1=6.4571, respectively. It is observed that the motion is of a periodic type at small forcing amplitudes. Nonetheless, different dynamic responses involving period-2, period-4 and chaos are observed for the nanofluid-conveying NSGT nanotube for larger forcing amplitudes. Figure 9 reveals the motion characteristics at F_1=45.0 along both *x* and *z* directions; the nanotube exhibits a periodic response.

Figure 10 indicates the influences of increasing imperfection on the scale-dependent response of fluid-conveying NSGT tubes; A_0=0.05, ω_1= 8.0937 and U = 4.90. Although the dynamic response is of periodic type at small forcing amplitudes, a highly chaotic response is observed at larger forcing amplitudes. For example, Fig. 11 depicts the motion characteristics at F_1=38.0 along both *x* and *z* directions; the nanosystem exhibits a chaotic response for this large forcing amplitude. This is owing to the fact that large forcing amplitudes cause more chaos in the mechanical response of the nanoscale system. Comparing Figs. 8 and 10 shows that when

the imperfection amplitude increases from A_0=0.01 to A_0=0.05, the dynamic response becomes more chaotic. It means that large initial deflections lead to a significant increase in the chance of observing chaos in the mechanical behaviour of nanotubes conveying nanofluid since large initial deflections make the nanotube weaker and less stable.

To study the effect of increasing fluid velocity on the bifurcation behaviour of nanofluid-conveying NSGT nanotubes, Fig. 12 is plotted; the imperfection amplitude is set to A_0=0.0 whereas the nanofluid speed is U = 5.00. For large forcing amplitudes, the NSGT nanotube exhibits a periodic motion while different motion types are seen for smaller ones. Furthermore, making a comparison between Figs. 4 and 12 shows that when the nanofluid speed is slightly increased, chaotic regions shift towards smaller forcing amplitudes. This is because of the fact that when there is a fluid-conveying tube subject to a constant applied load, chaos is observed earlier in the system by increasing the fluid speed.

Figure 13 is aimed at illustrating the bifurcation behaviour of nanofluid-conveying NSGT nanotubes for the size-dependent dynamics along both x and z directions; the imperfection amplitude is not zero (A_0=0.005) while the nanofluid speed is the same as the previous figure (i.e. U = 5). The natural frequency is computed as ω_1=5.8362. A small imperfection in the geometry of the NSGT nanotube remarkably alters the bifurcation behaviour. Take into account point F_1=40 as a salient example of this alteration. The motion type is period-5 at this point for A_0=0.005, as shown in Fig. 14, while it is chaotic for the case without geometric imperfection.

The influences of increasing geometrical imperfection on the bifurcation behaviour is also highlighted in Fig. 15; A_0=0.01, ω_1=7.1186 and U = 5.00. It is seen that the chaotic regions shift

towards larger forcing amplitudes with increasing the imperfection amplitude from A_0=0.005 to A_0=0.01 for U = 5.00. Moreover, the mechanical response of the nanotube is more chaotic for larger values of F_1 since higher transverse loads cause more chaos in the fluid-conveying tube at nanoscales. To provide the reader with more data about the dynamics of NSGT nanotubes analysed in the previous figure, Fig. 16 is plotted. It is found that the nanotube displays a highly chaotic behaviour at F_1=49.2.

Figure 17 is plotted to study the effects of nonlocal and strain gradient parameters on the bifurcations and chaos of fluid-conveying nanotubes. The dimensionless geometric imperfection and fluid velocity are A_0=0.01 and U = 5.00, respectively. It is observed that strain gradient effects decrease chaos in the nanosystem (compare Fig. 17(c) with Fig. 17(a)) whereas nonlocal effects lead to a substantial increase in the chaotic region (compare Fig. 17(b) with Fig. 17(a)). This is because enhancing nonlocal effects reduces the structural stiffness whereas the strain gradient coefficient leads to the opposite influence. Various elasticity theories are also compared in this figure; NET, CET and SGT stand for the nonlocal, classical and strain gradient elasticity theories, respectively. The SGT is not able to describe chaos in the nanosystem while the NET overestimates the chaotic region.

5. Conclusions

A nonlinear continuum-based analysis has been conducted on the chaotic behaviour of nanofluid-conveying NSGT nanotubes with an initial deflection. To simulate the influences of the relative motion between the nanofluid and nanotube at the interface, the Beskok-Karniadakis model was used. The nonlinear differential equations were derived according to an energy-work balance technique. Furthermore, a direct-time-integration approach and a Galerkin scheme were used for extracting the size-dependent mechanical response of the NSGT nanosystem incorporating the influences of a geometric imperfection. For NSGT nanotubes without an initial deflection, the motion is of a periodic type at small forcing amplitudes whereas a highly chaotic behaviour is observed as the forcing amplitude is increased. Implementing a small initial deflection first reduces chaotic response of the nanofluid-conveying NSGT nanotube. However, the dynamic response becomes more chaotic when the imperfection amplitude further increases. In addition, chaotic regions shift towards smaller forcing amplitudes as the nanofluid speed is slightly increased.

References

[1] C. Demir, Ö. Civalek, Torsional and longitudinal frequency and wave response of microtubules based on the nonlocal continuum and nonlocal discrete models, Applied Mathematical Modelling, 37 (2013) 9355-9367.
[2] Ö. Civalek, Ç. Demir, Bending analysis of microtubules using nonlocal Euler–Bernoulli beam theory, Applied Mathematical Modelling, 35 (2011) 2053-2067.
[3] M. Bedroud, R. Nazemnezhad, S. Hosseini-Hashemi, M. Valixani, Buckling of FG circular/annular Mindlin nanoplates with an internal ring support using nonlocal elasticity, Applied Mathematical Modelling, 40 (2016) 3185-3210.
[4] J. Liu, C. Li, X. Fan, L. Tong, Transverse free vibration and stability of axially moving nanoplates based on nonlocal elasticity theory, Applied Mathematical Modelling, 45 (2017) 65-84.
[5] A. Assadi, B. Farshi, Stability analysis of graphene based laminated composite sheets under non-uniform inplane loading by nonlocal elasticity, Applied Mathematical Modelling, 35 (2011) 4541-4549.
[6] M.H. Ghayesh, Nonlinear vibration analysis of axially functionally graded shear-deformable tapered beams, Applied Mathematical Modelling, 59 (2018) 583-596.
[7] S. Hosseini-Hashemi, R. Nazemnezhad, M. Bedroud, Surface effects on nonlinear free vibration of functionally graded nanobeams using nonlocal elasticity, Applied Mathematical Modelling, 38 (2014) 3538-3553.
[8] W. Yang, W. Kang, X. Wang, Thermal and surface effects on the pull-in characteristics of circular nanoplate NEMS actuator based on nonlocal elasticity theory, Applied Mathematical Modelling, 43 (2017) 321-336.
[9] J. Sun, Z. Wang, Z. Zhou, X. Xu, C. Lim, Surface effects on the buckling behaviors of piezoelectric cylindrical nanoshells using nonlocal continuum model, Applied Mathematical Modelling, 59 (2018) 341-356.
[10] J. Peng, L. Yang, F. Lin, J. Yang, Dynamic analysis of size-dependent micro-beams with nonlinear elasticity under electrical actuation, Applied Mathematical Modelling, 43 (2017) 441-453.
[11] M. Aydogdu, A nonlocal rod model for axial vibration of double-walled carbon nanotubes including axial van der Waals force effects, Journal of Vibration and Control, 21 (2015) 3132-3154.
[12] M. Aydogdu, I. Elishakoff, On the vibration of nanorods restrained by a linear spring in-span, Mechanics Research Communications, 57 (2014) 90-96.
[13] M. Farajpour, A. Shahidi, F. Tabataba'i-Nasab, A. Farajpour, Vibration of initially stressed carbon nanotubes under magneto-thermal environment for nanoparticle delivery via higher-order nonlocal strain gradient theory, The European Physical Journal Plus, 133 (2018) 219.
[14] M. Aydogdu, Longitudinal wave propagation in multiwalled carbon nanotubes, Composite Structures, 107 (2014) 578-584.
[15] C. Li, A nonlocal analytical approach for torsion of cylindrical nanostructures and the existence of higher-order stress and geometric boundaries, Composite Structures, 118 (2014) 607-621.
[16] C. Li, L. Yao, W. Chen, S. Li, Comments on nonlocal effects in nano-cantilever beams, International Journal of Engineering Science, 87 (2015) 47-57.
[17] C. Li, S. Lai, X. Yang, On the nano-structural dependence of nonlocal dynamics and its relationship to the upper limit of nonlocal scale parameter, Applied Mathematical Modelling, 69 (2019) 127-141.
[18] B. Akgöz, Ö. Civalek, A new trigonometric beam model for buckling of strain gradient microbeams, International Journal of Mechanical Sciences, 81 (2014) 88-94.
[19] A.G. Shenas, P. Malekzadeh, Free vibration of functionally graded quadrilateral microplates in thermal environment, Thin-Walled Structures, 106 (2016) 294-315.
[20] P. Malekzadeh, A.G. Shenas, S. Ziaee, Thermal buckling of functionally graded triangular microplates, Journal of the Brazilian Society of Mechanical Sciences and Engineering, 40 (2018) 418.

[21] B. Akgöz, Ö. Civalek, Application of strain gradient elasticity theory for buckling analysis of protein microtubules, Current Applied Physics, 11 (2011) 1133-1138.
[22] H. Ma, X.-L. Gao, J. Reddy, A microstructure-dependent Timoshenko beam model based on a modified couple stress theory, Journal of the Mechanics and Physics of Solids, 56 (2008) 3379-3391.
[23] M.H. Ghayesh, H. Farokhi, Parametric instability of microbeams in supercritical regime, Nonlinear Dynamics, 83 (2016) 1171-1183.
[24] A.M. Dehrouyeh-Semnani, A. Bahrami, On size-dependent Timoshenko beam element based on modified couple stress theory, International Journal of Engineering Science, 107 (2016) 134-148.
[25] A.M. Dehrouyeh-Semnani, M. Nikkhah-Bahrami, M.R.H. Yazdi, On nonlinear stability of fluid-conveying imperfect micropipes, International Journal of Engineering Science, 120 (2017) 254-271.
[26] H. Farokhi, M.H. Ghayesh, Nonlinear mechanical behaviour of microshells, International Journal of Engineering Science, 127 (2018) 127-144.
[27] H. Farokhi, M.H. Ghayesh, Viscoelastic shear deformable microplates: Nonlinear forced resonant characteristics, Mechanical Systems and Signal Processing, 118 (2019) 742-756.
[28] C. Lim, G. Zhang, J. Reddy, A higher-order nonlocal elasticity and strain gradient theory and its applications in wave propagation, Journal of the Mechanics and Physics of Solids, 78 (2015) 298-313.
[29] X. Li, L. Li, Y. Hu, Z. Ding, W. Deng, Bending, buckling and vibration of axially functionally graded beams based on nonlocal strain gradient theory, Composite Structures, 165 (2017) 250-265.
[30] A. Farajpour, M.H. Yazdi, A. Rastgoo, M. Mohammadi, A higher-order nonlocal strain gradient plate model for buckling of orthotropic nanoplates in thermal environment, Acta Mechanica, 227 (2016) 1849-1867.
[31] L. Wang, Q. Ni, On vibration and instability of carbon nanotubes conveying fluid, Computational Materials Science, 43 (2008) 399-402.
[32] P. Soltani, M. Taherian, A. Farshidianfar, Vibration and instability of a viscous-fluid-conveying single-walled carbon nanotube embedded in a visco-elastic medium, Journal of Physics D: Applied Physics, 43 (2010) 425401.
[33] H.-L. Lee, W.-J. Chang, Free transverse vibration of the fluid-conveying single-walled carbon nanotube using nonlocal elastic theory, Journal of Applied Physics, 103 (2008) 024302.
[34] H. Zeighampour, Y.T. Beni, Size-dependent vibration of fluid-conveying double-walled carbon nanotubes using couple stress shell theory, Physica E: Low-dimensional Systems and Nanostructures, 61 (2014) 28-39.
[35] Y.-X. Zhen, B. Fang, Y. Tang, Thermal–mechanical vibration and instability analysis of fluid-conveying double walled carbon nanotubes embedded in visco-elastic medium, Physica E: Low-dimensional Systems and Nanostructures, 44 (2011) 379-385.
[36] F. Liang, Y. Su, Stability analysis of a single-walled carbon nanotube conveying pulsating and viscous fluid with nonlocal effect, Applied Mathematical Modelling, 37 (2013) 6821-6828.
[37] Z.K. Maraghi, A.G. Arani, R. Kolahchi, S. Amir, M. Bagheri, Nonlocal vibration and instability of embedded DWBNNT conveying viscose fluid, Composites Part B: Engineering, 45 (2013) 423-432.
[38] S. Oveissi, D. Toghraie, S.A. Eftekhari, Longitudinal vibration and stability analysis of carbon nanotubes conveying viscous fluid, Physica E: Low-dimensional Systems and Nanostructures, 83 (2016) 275-283.
[39] H. Askari, E. Esmailzadeh, Forced vibration of fluid conveying carbon nanotubes considering thermal effect and nonlinear foundations, Composites Part B: Engineering, 113 (2017) 31-43.
[40] L. Li, Y. Hu, Wave propagation in fluid-conveying viscoelastic carbon nanotubes based on nonlocal strain gradient theory, Computational materials science, 112 (2016) 282-288.
[41] A. Ghasemi, M. Dardel, M.H. Ghasemi, M.M. Barzegari, Analytical analysis of buckling and post-buckling of fluid conveying multi-walled carbon nanotubes, Applied Mathematical Modelling, 37 (2013) 4972-4992.

[42] H. Mohammadi, M. Mahzoon, M. Mohammadi, M. Mohammadi, Postbuckling instability of nonlinear nanobeam with geometric imperfection embedded in elastic foundation, Nonlinear Dynamics, 76 (2014) 2005-2016.
[43] M.H. Ghayesh, H. Farokhi, A. Gholipour, Vibration analysis of geometrically imperfect three-layered shear-deformable microbeams, International Journal of Mechanical Sciences, 122 (2017) 370-383.
[44] A. Beskok, G.E. Karniadakis, Report: a model for flows in channels, pipes, and ducts at micro and nano scales, Microscale Thermophysical Engineering, 3 (1999) 43-77.
[45] A. Farajpour, M.H. Ghayesh, H. Farokhi, A review on the mechanics of nanostructures, International Journal of Engineering Science, 133 (2018) 231-263.
[46] A. Hadi, M.Z. Nejad, M. Hosseini, Vibrations of three-dimensionally graded nanobeams, International Journal of Engineering Science, 128 (2018) 12-23.
[47] M.Z. Nejad, A. Hadi, Eringen's non-local elasticity theory for bending analysis of bi-directional functionally graded Euler–Bernoulli nano-beams, International Journal of Engineering Science, 106 (2016) 1-9.
[48] A. Farajpour, A. Rastgoo, M. Farajpour, Nonlinear buckling analysis of magneto-electro-elastic CNT-MT hybrid nanoshells based on the nonlocal continuum mechanics, Composite Structures, 180 (2017) 179-191.
[49] L. Li, Y. Hu, L. Ling, Wave propagation in viscoelastic single-walled carbon nanotubes with surface effect under magnetic field based on nonlocal strain gradient theory, Physica E: Low-dimensional Systems and Nanostructures, 75 (2016) 118-124.
[50] M.R. Farajpour, A. Rastgoo, A. Farajpour, M. Mohammadi, Vibration of piezoelectric nanofilm-based electromechanical sensors via higher-order non-local strain gradient theory, Micro & Nano Letters, 11 (2016) 302-307.
[51] L. Li, H. Tang, Y. Hu, The effect of thickness on the mechanics of nanobeams, International Journal of Engineering Science, 123 (2018) 81-91.
[52] H. Tang, L. Li, Y. Hu, Coupling effect of thickness and shear deformation on size-dependent bending of micro/nano-scale porous beams, Applied Mathematical Modelling, 66 (2019) 527-547.
[53] H. Tang, L. Li, Y. Hu, W. Meng, K. Duan, Vibration of nonlocal strain gradient beams incorporating Poisson's ratio and thickness effects, Thin-Walled Structures, 137 (2019) 377-391.
[54] M. Şimşek, Nonlinear free vibration of a functionally graded nanobeam using nonlocal strain gradient theory and a novel Hamiltonian approach, International Journal of Engineering Science, 105 (2016) 12-27.
[55] A. Farajpour, M.H. Ghayesh, H. Farokhi, Large-amplitude coupled scale-dependent behaviour of geometrically imperfect NSGT nanotubes, International Journal of Mechanical Sciences, 150 (2019) 510-525.
[56] M.H. Ghayesh, A. Farajpour, Nonlinear mechanics of nanoscale tubes via nonlocal strain gradient theory, International Journal of Engineering Science, 129 (2018) 84-95.
[57] L. Li, Y. Hu, Nonlinear bending and free vibration analyses of nonlocal strain gradient beams made of functionally graded material, International Journal of Engineering Science, 107 (2016) 77-97.
[58] M.H. Ghayesh, Functionally graded microbeams: Simultaneous presence of imperfection and viscoelasticity, International Journal of Mechanical Sciences, 140 (2018) 339-350.
[59] M.H. Ghayesh, Viscoelastic dynamics of axially FG microbeams, International Journal of Engineering Science, 135 (2019) 75-85.
[60] H. Farokhi, M.H. Ghayesh, A. Gholipour, S. Hussain, Resonant responses of three-layered shear-deformable microbeams, Microsystem Technologies, 24 (2018) 2123-2136.
[61] L. Li, Y. Hu, X. Li, L. Ling, Size-dependent effects on critical flow velocity of fluid-conveying microtubes via nonlocal strain gradient theory, Microfluidics and Nanofluidics, 20 (2016) 76.

[62] H. Dai, L. Wang, A. Abdelkefi, Q. Ni, On nonlinear behavior and buckling of fluid-transporting nanotubes, International Journal of Engineering Science, 87 (2015) 13-22.

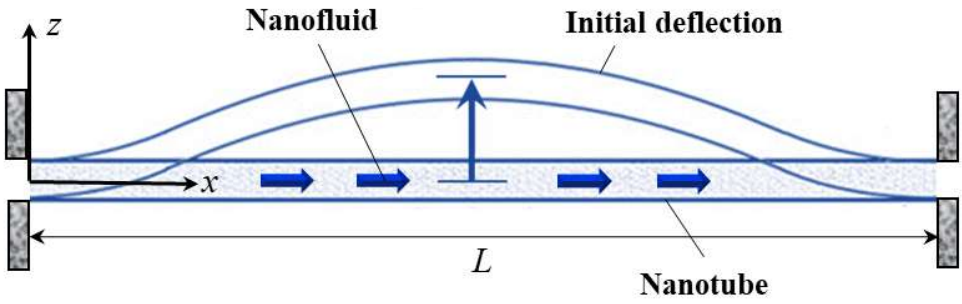

Figure 1: A nanofluid-conveying NSGT nanotube with an initial deflection.

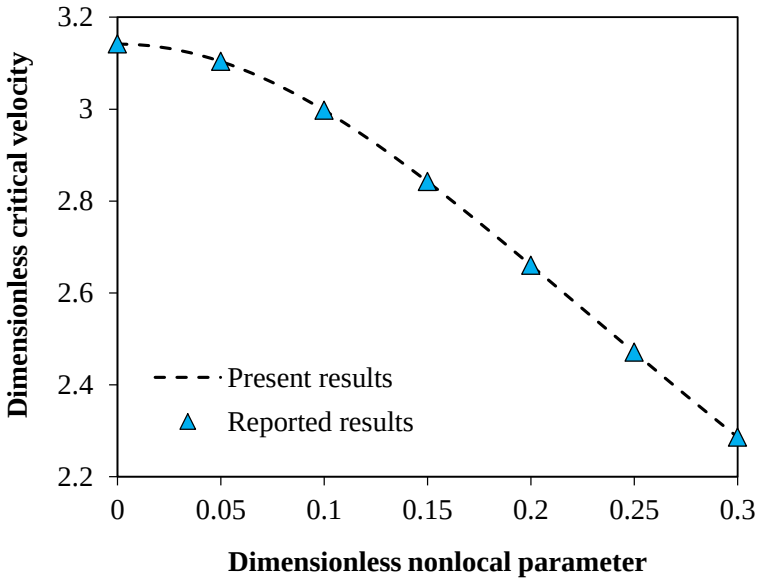

Figure 2: Verification study for the size-dependent modelling; reported results are from Refs. [61, 62].

(a)

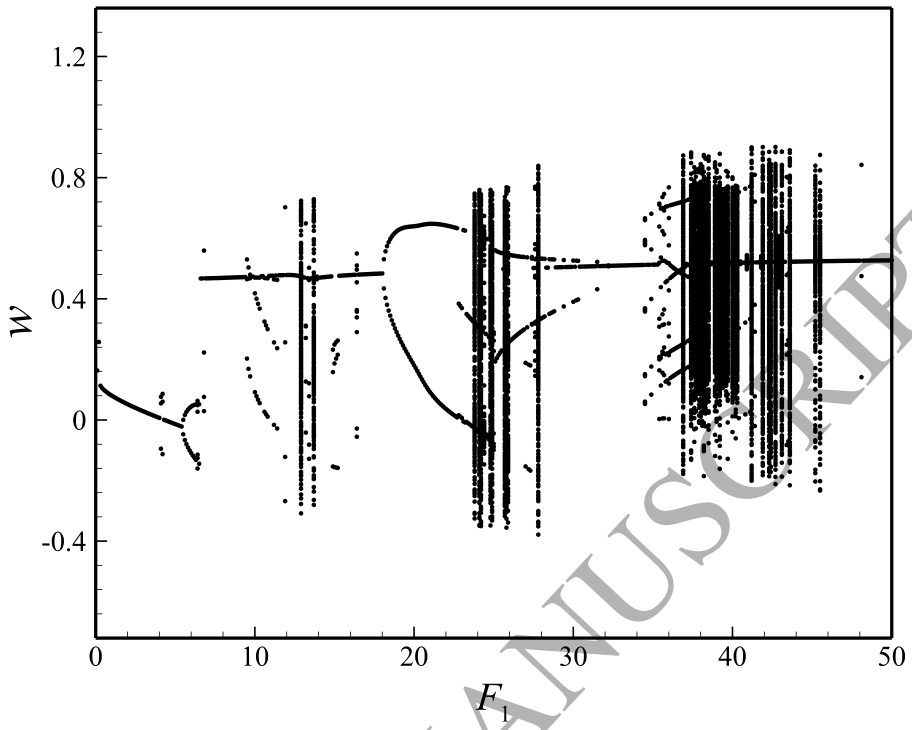

(b)

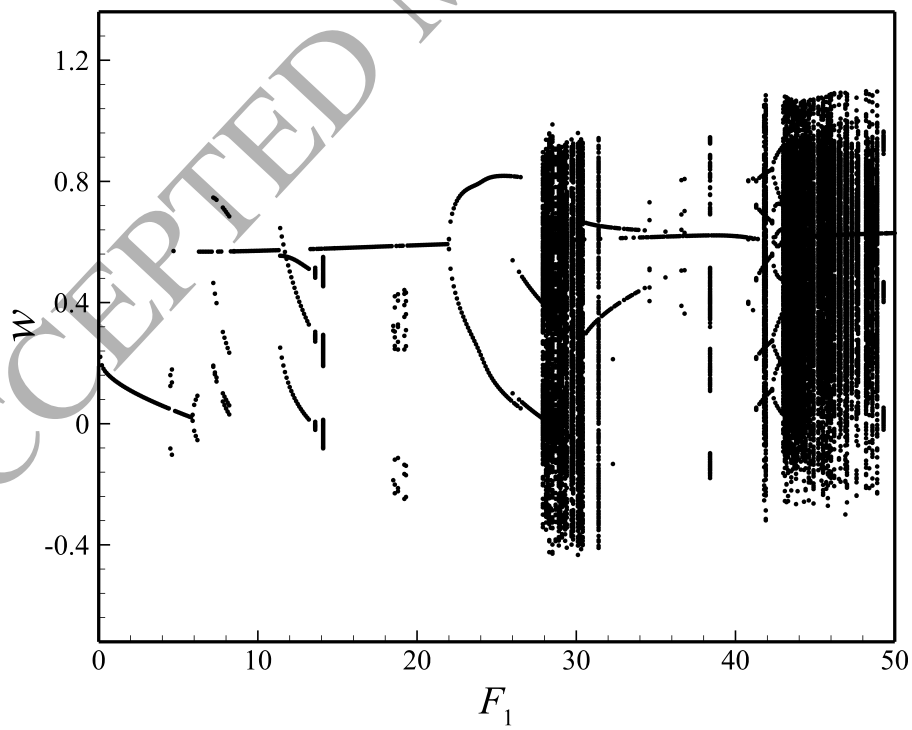

(c)

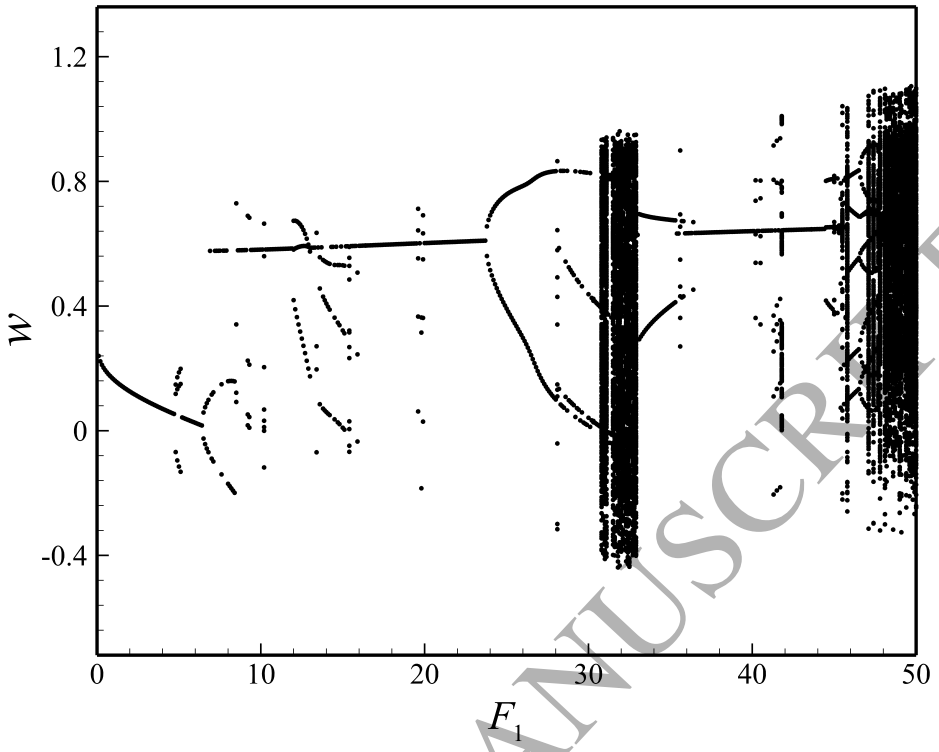

(d)

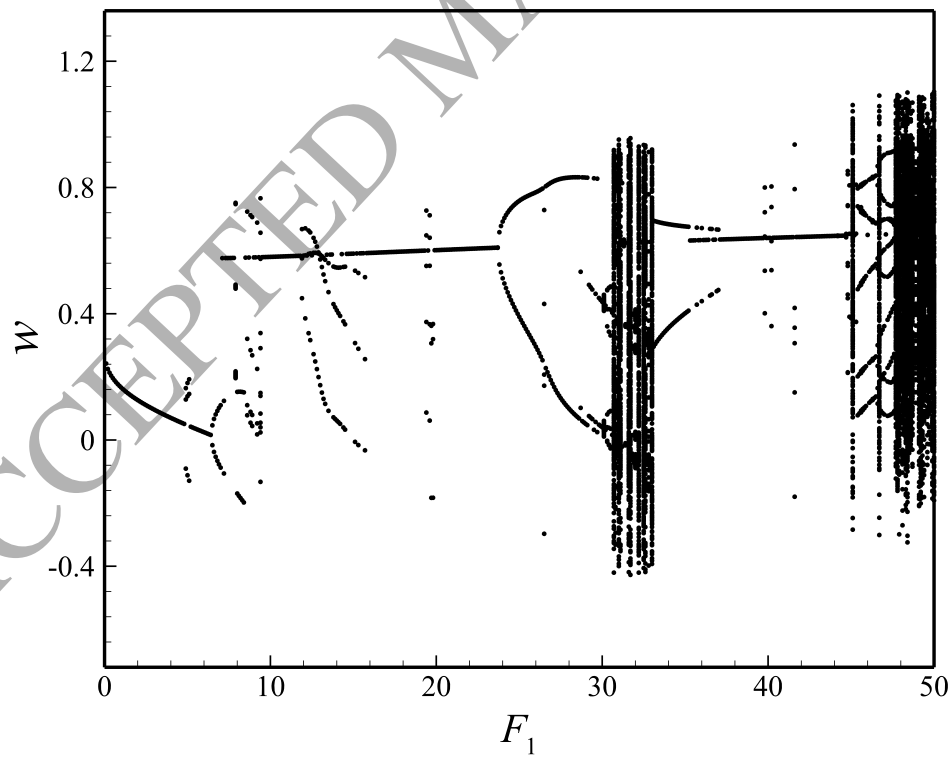

Figure 3: Convergence analysis of the bifurcation behaviour of nanofluid-conveying NSGT nanotubes for the transverse motion: (a) 4-DOF; (b) 8-DOF; (c) 16-DOF; (d) 20-DOF.

(a)

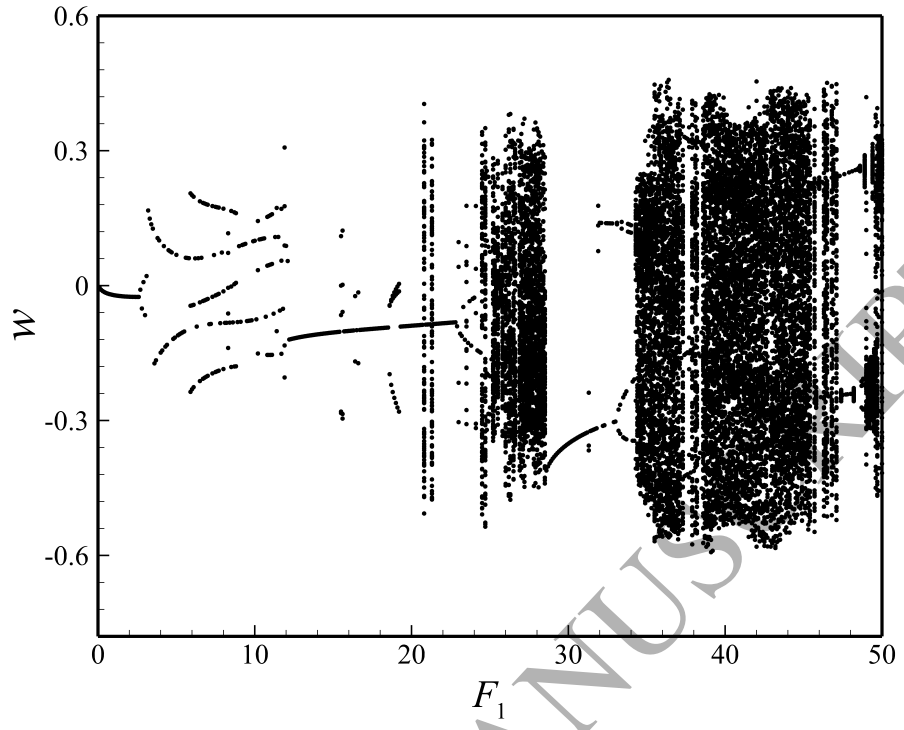

(b)

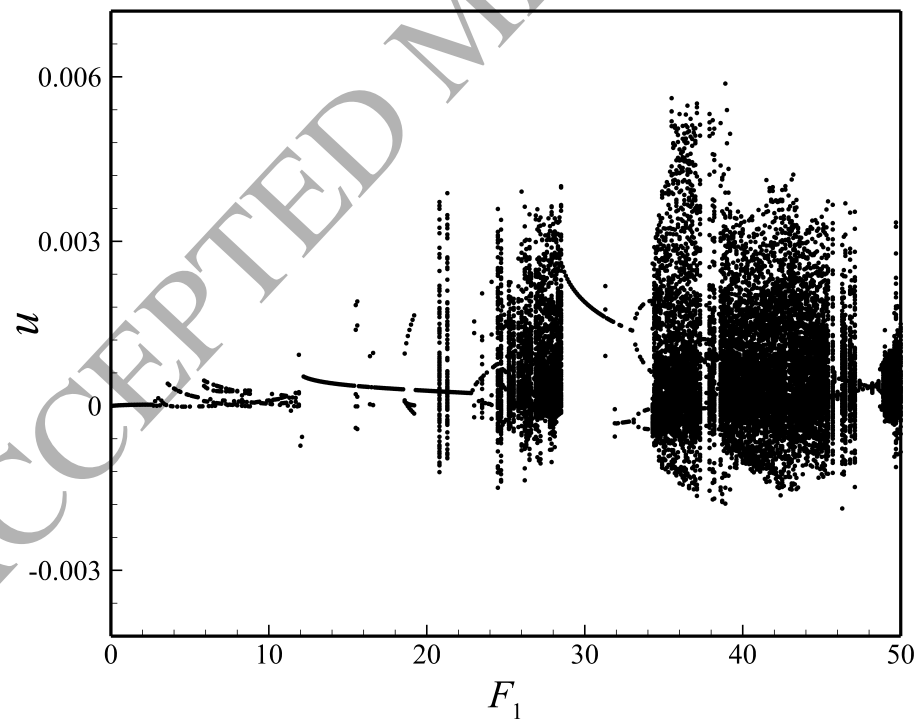

Figure 4: Bifurcation of fluid-conveying NSGT tubes: (a) motion in transverse axis (x=0.50); (b) motion in longitudinal axis (x=0.65); A_0=0, ω_1= 2.1837, and U = 4.90.

(a)

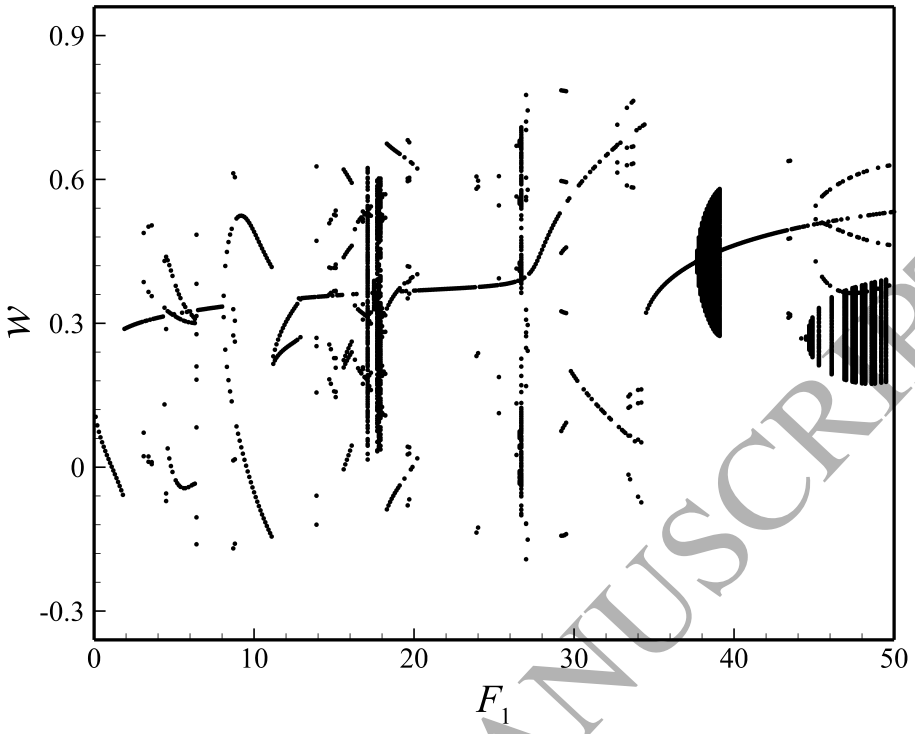

(b)

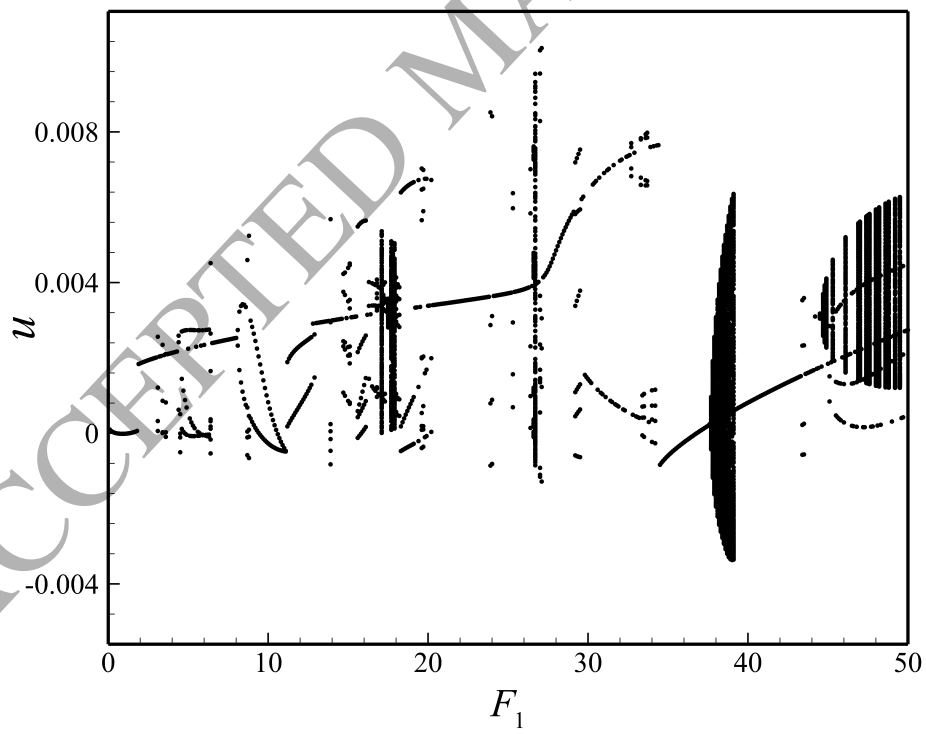

Figure 5: Bifurcation of fluid-conveying NSGT tubes: (a) motion in transverse axis (x=0.50); (b) motion in longitudinal axis (x=0.65); A_0=0.005, ω_1= 4.9808 and U = 4.90.

(a)

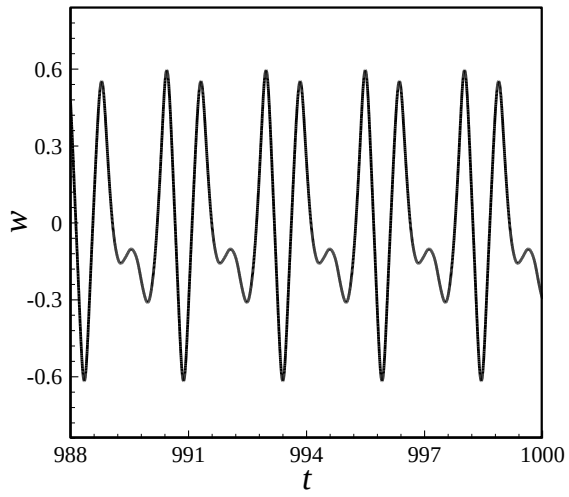

(b)

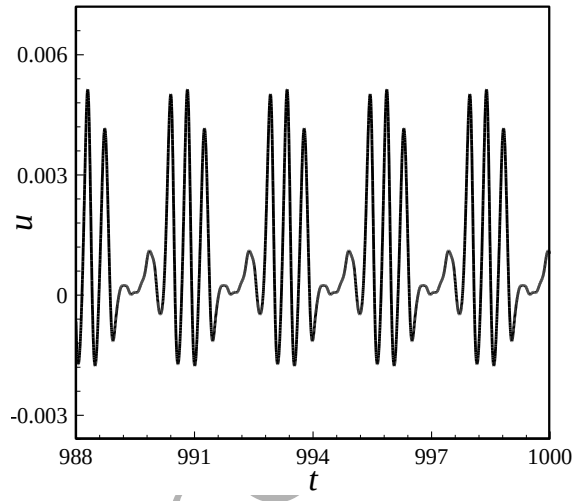

(c)

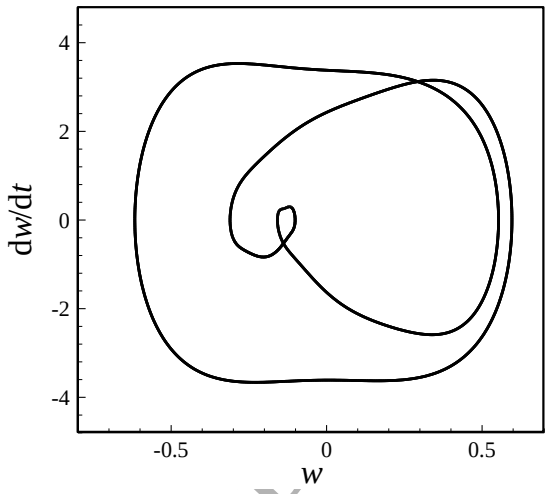

(d)

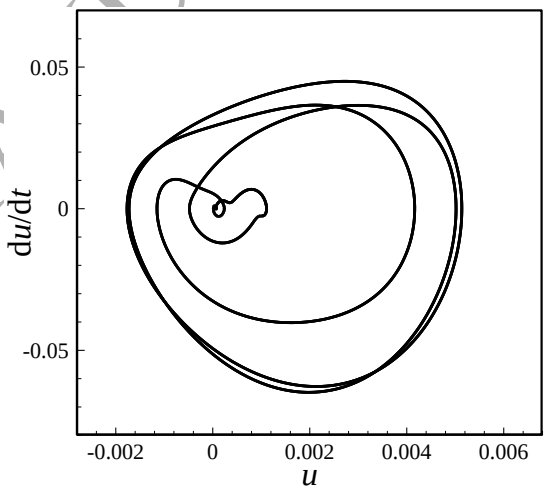

(e)

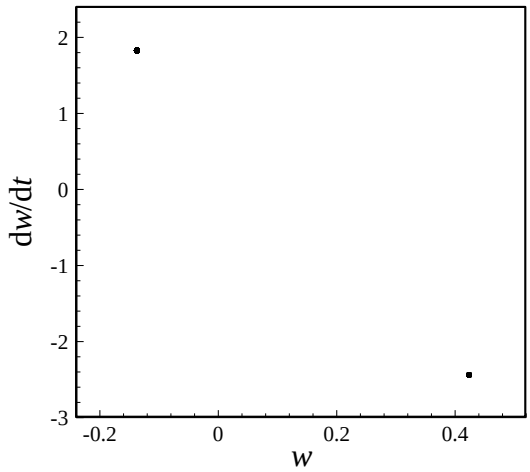

(f)

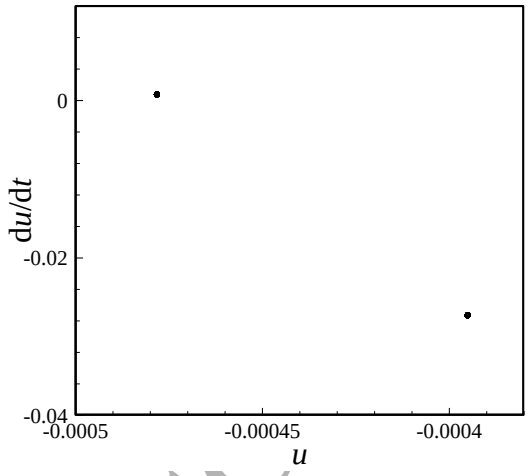

Figure 6: Motion characteristics at F_1=11.0 for the NSGT nanotube analysed in Fig. 3: (a) $w[x=0.5]$ against time; (b) $u\left[x=0.65\right]$ against time; phase-plane diagram for (c) $w[x=0.5]$ and (d) $u\left[x=0.65\right]$; Poincaré section for (e) $w[x=0.5]$ and (d) $u\left[x=0.65\right]$.

(a)

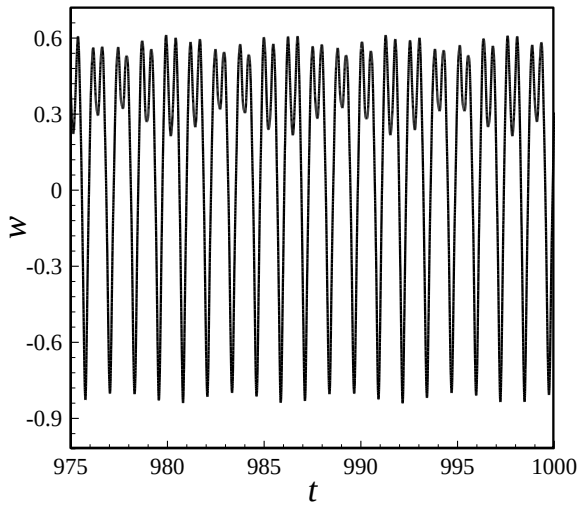

(b)

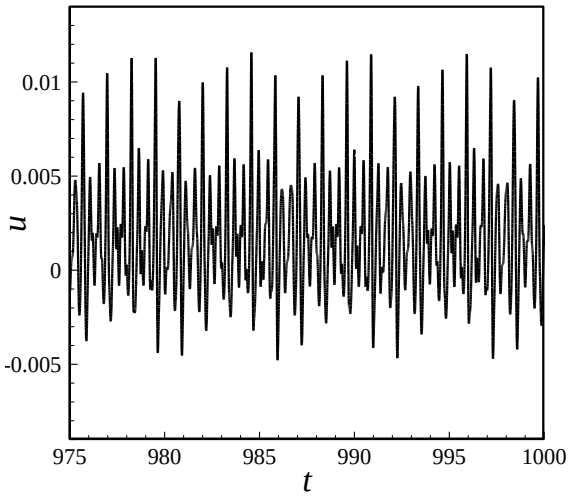

(c)

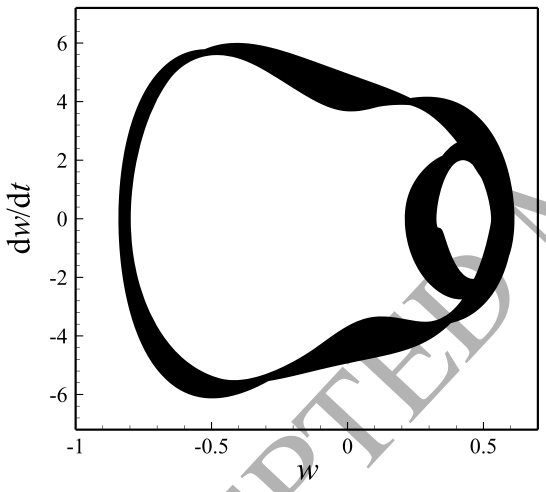

(d)

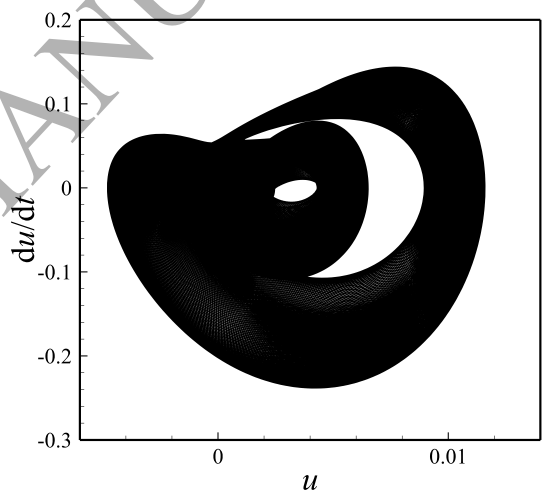

(e)

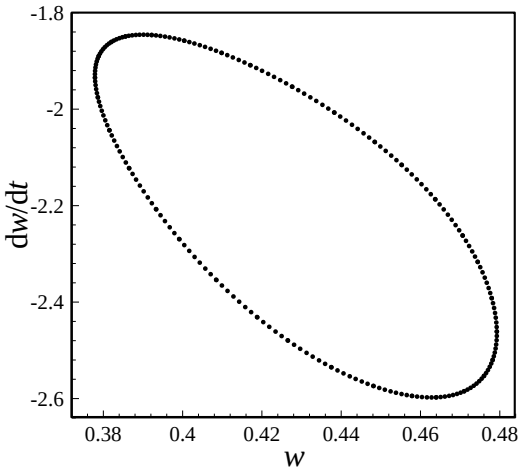

(f)

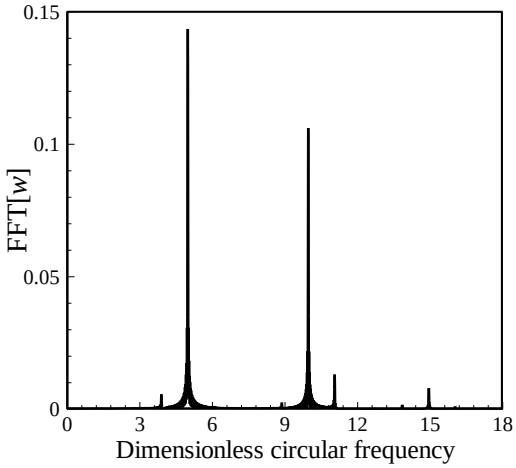

Figure 7: Motion characteristics at F_1=37.8 for the NSGT nanotube analysed in Fig. 3: (a) $w\left[x=0.5\right]$ against time; (b) $u\left[x=0.65\right]$ against time; phase-plane diagram for (c) $w\left[x=0.5\right]$ and (d) $u\left[x=0.65\right]$; (e) Poincaré section for $w\left[x=0.5\right]$; (f) FFT for $w\left[x=0.5\right]$.

(a)

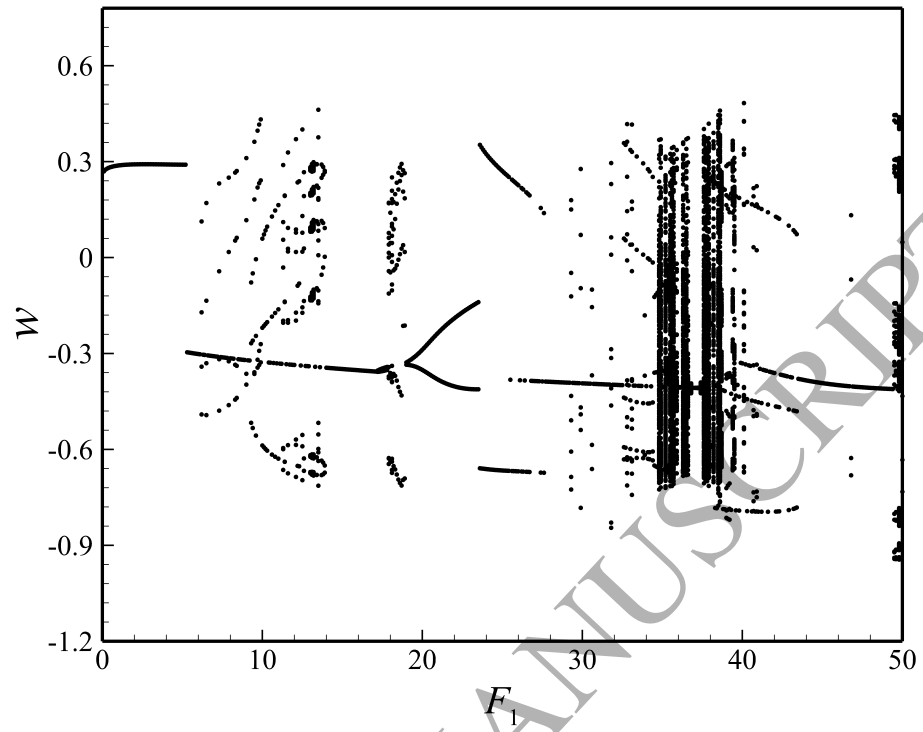

(b)

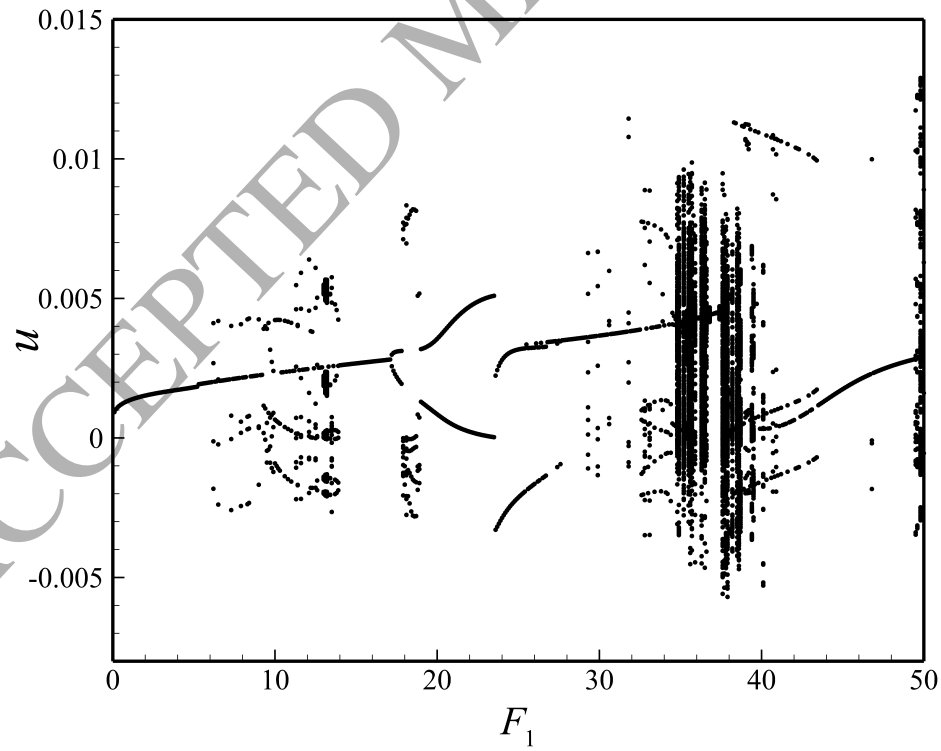

Figure 8: Bifurcation of fluid-conveying NSGT tubes: (a) motion in transverse axis (x=0.50); (b) motion in longitudinal axis (x=0.65); A_0=0.01, ω_1= 6.4571, and U = 4.90.

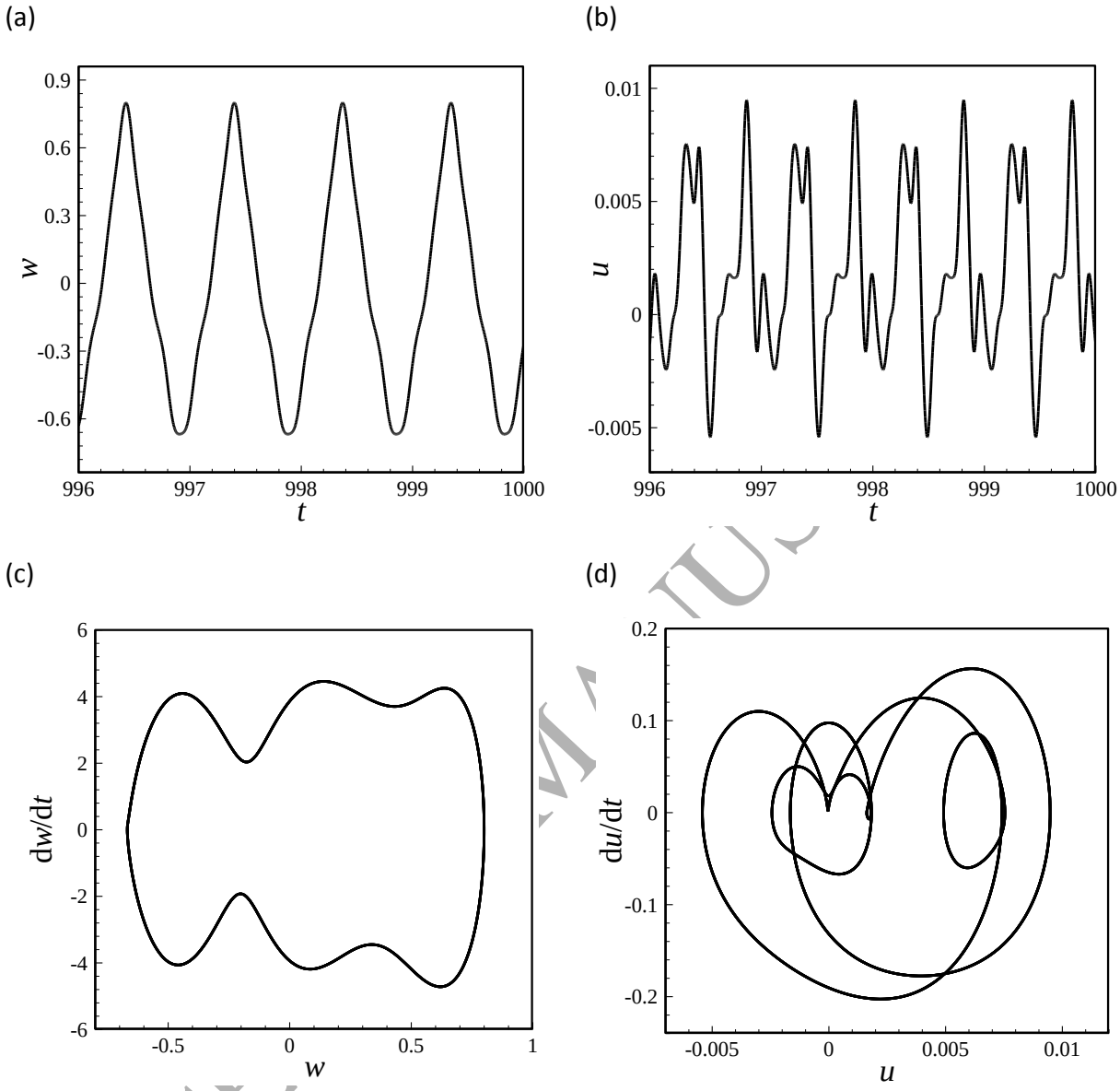

Figure 9: Motion characteristics at F_1=45.0 for the NSGT nanotube analysed in Fig. 6: (a) $w\left[x=0.5\right]$ against time; (b) $u\left[x=0.65\right]$ against time; phase-plane diagram for (c) $w[x=0.5]$ and (d) $u[x=0.65]$.

(a)

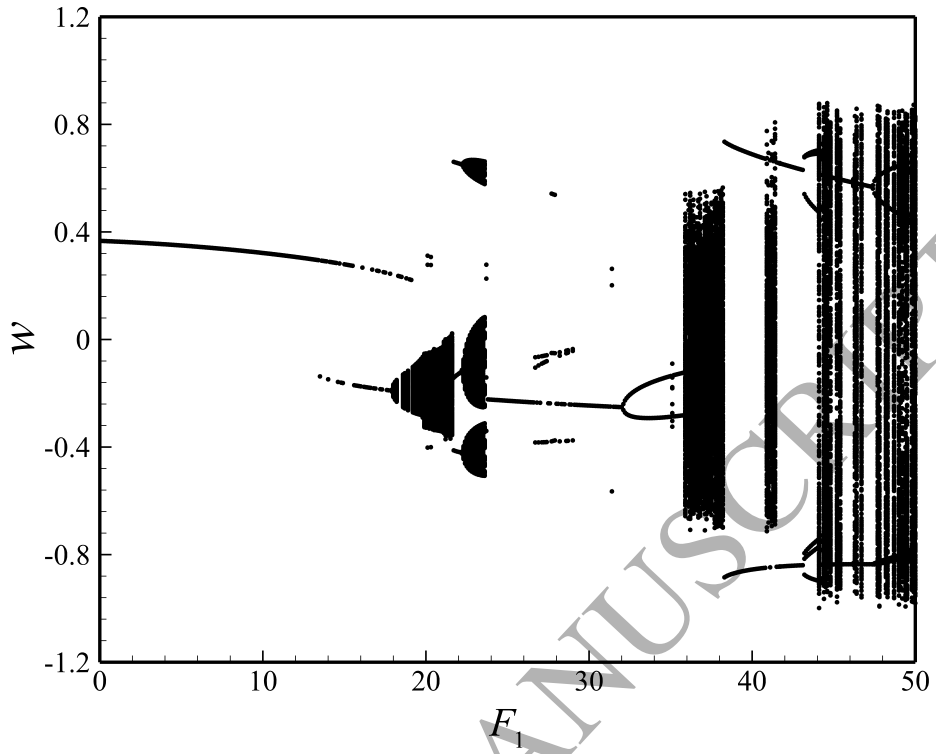

(b)

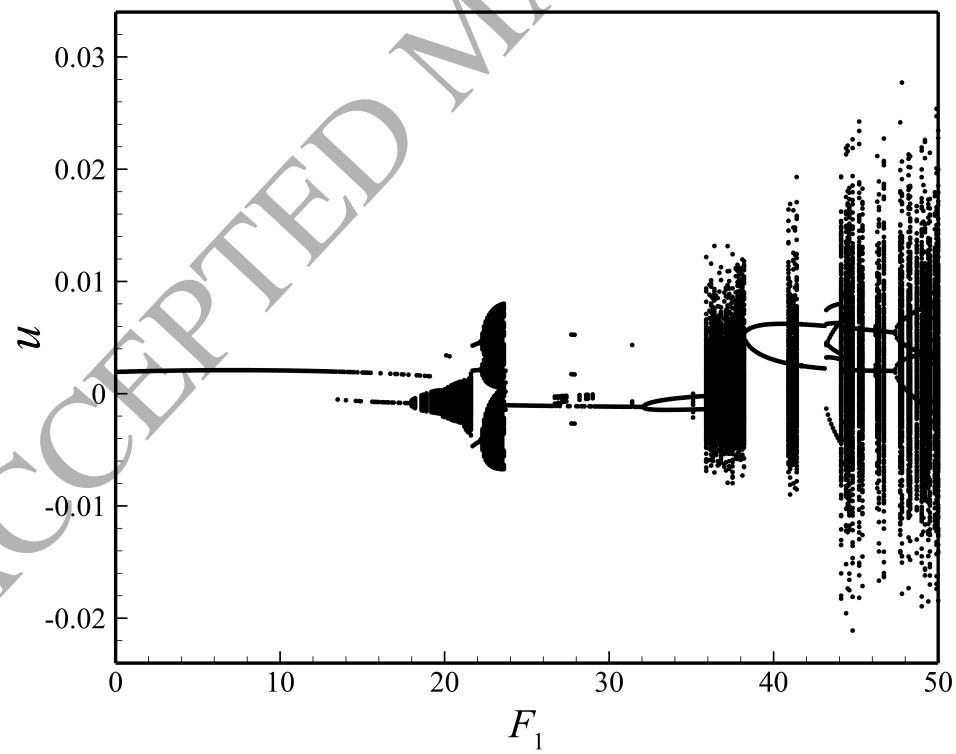

Figure 10: Bifurcation of fluid-conveying NSGT tubes: (a) motion in transverse axis (x=0.50); (b) motion in longitudinal axis (x=0.65); A_0=0.05, ω_1= 8.0937 and U = 4.90.

(a)

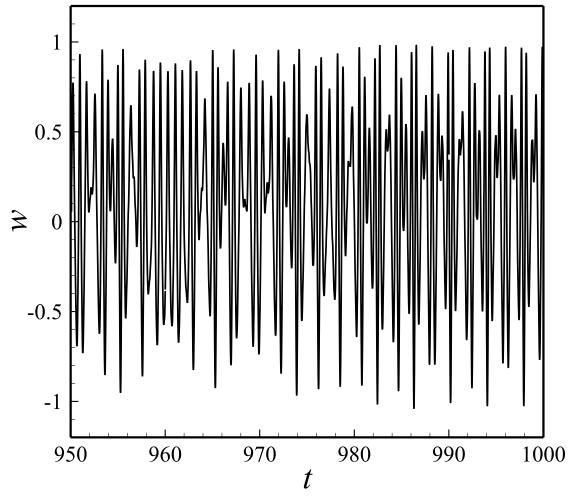

(b)

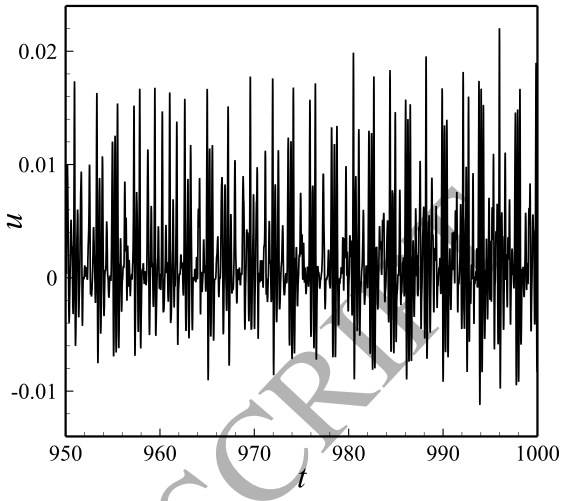

(c)

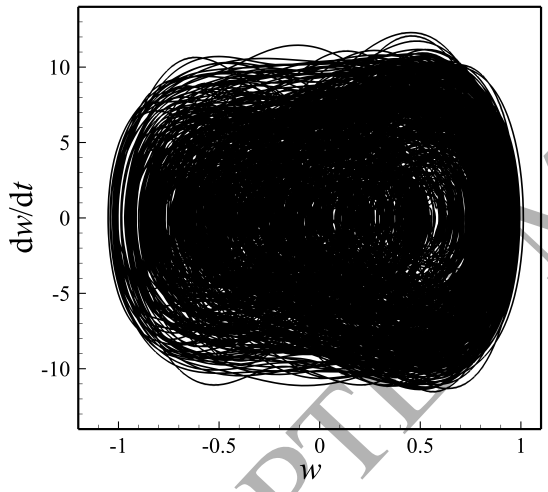

(d)

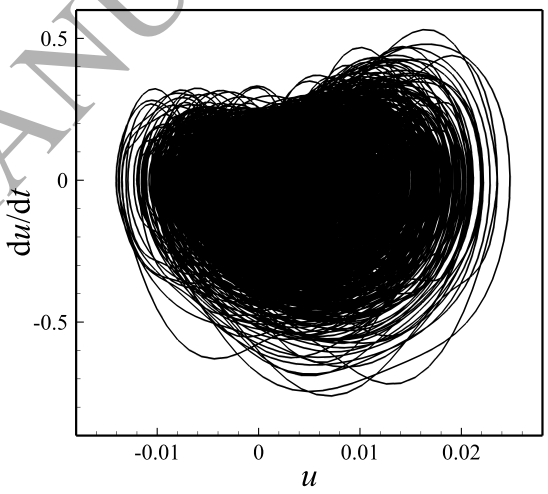

(e) (f)

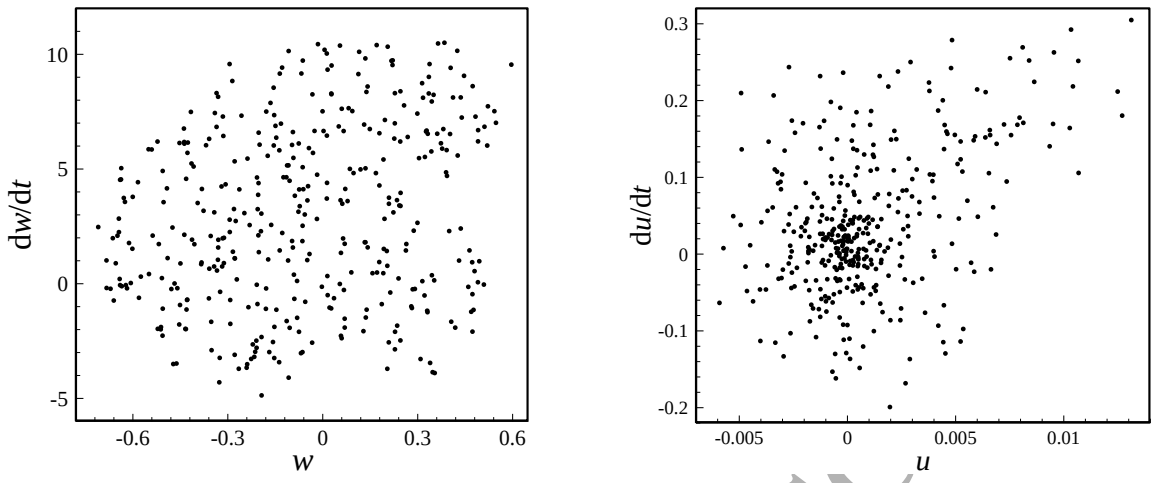

Figure 11: Motion characteristics at F_1=38.0 for the NSGT nanotube analysed in Fig. 8: (a) $w[x=0.5]$ against time; (b) $u[x=0.65]$ against time; phase-plane diagram for (c) $w[x=0.5]$ and (d) $u[x=0.65]$; Poincaré section for (e) $w[x=0.5]$ and (d) $u[x=0.65]$.

(a)

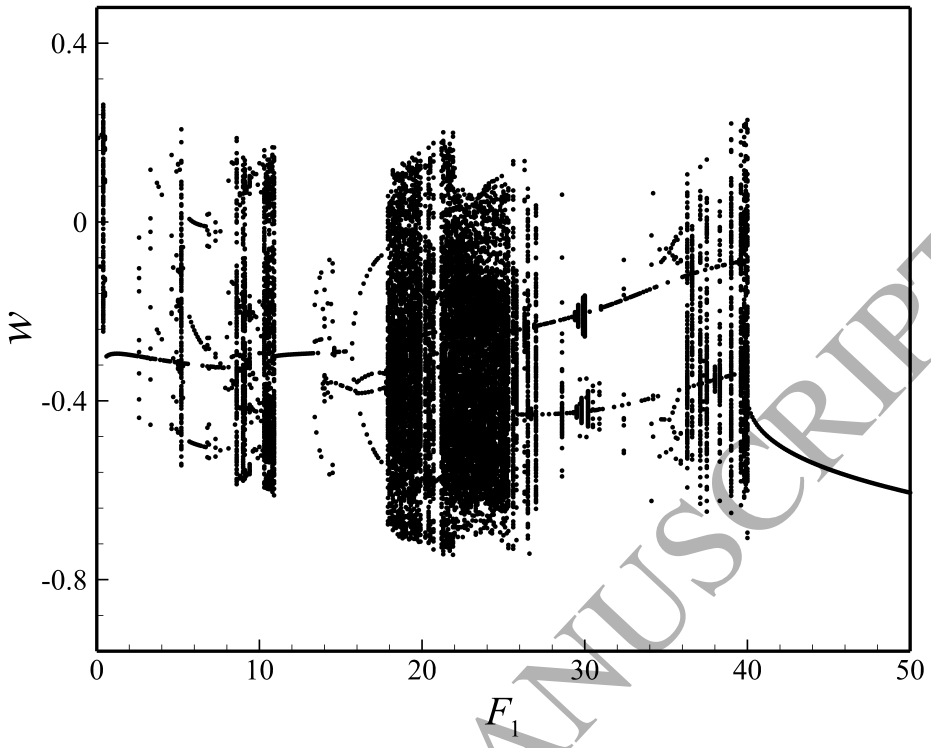

(b)

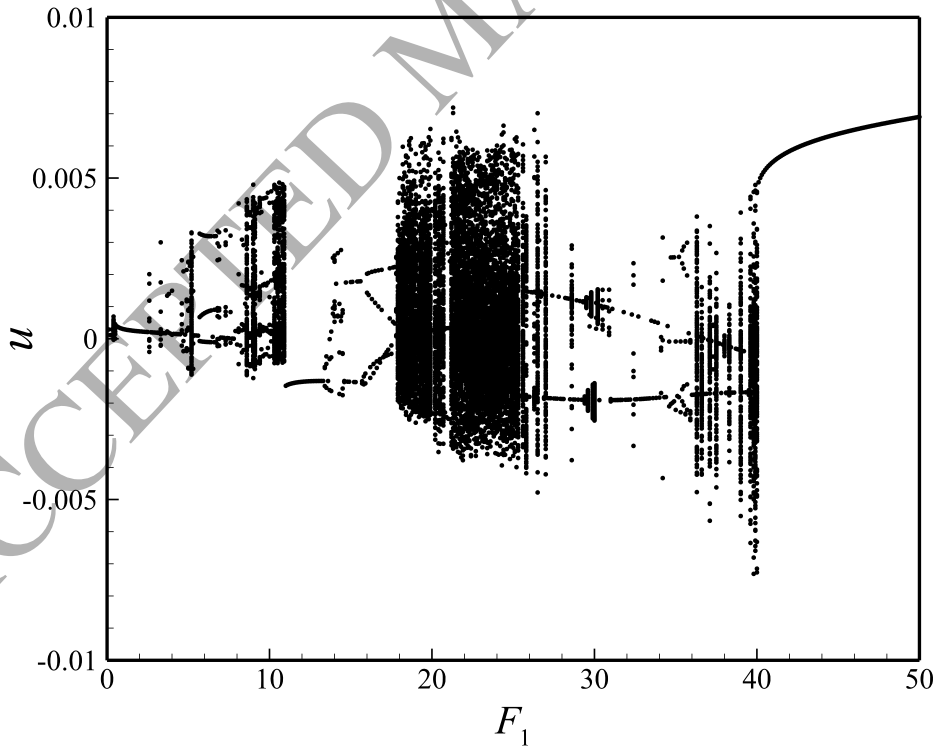

Figure 12: Bifurcation of fluid-conveying NSGT tubes: (a) motion in transverse axis (x=0.50); (b) motion in longitudinal axis (x=0.65); A_0=0.0, ω_1= 3.2546 and U= 5.00.

(a)

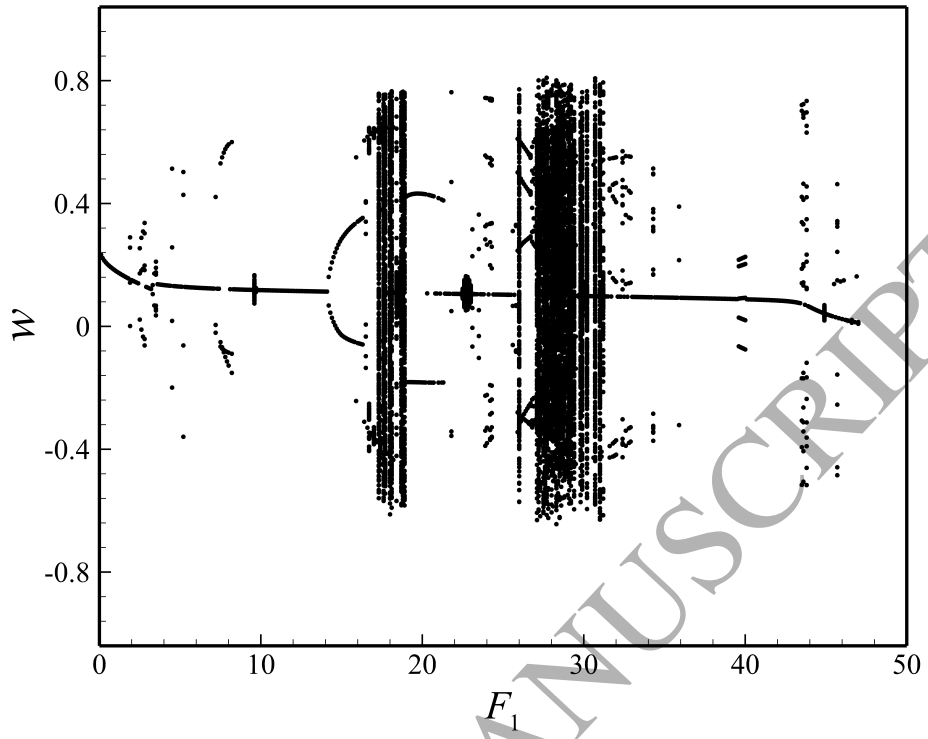

(b)

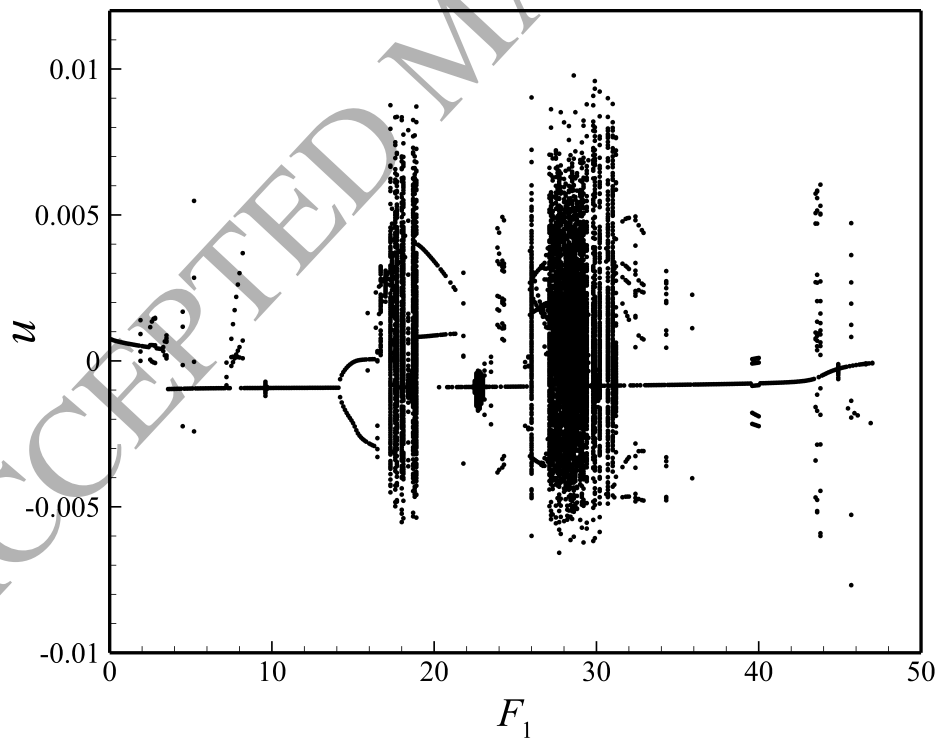

Figure 13: Bifurcation of fluid-conveying NSGT tubes: (a) motion in transverse axis (x=0.50); (b) motion in longitudinal axis (x=0.65); A_0=0.005, ω_1= 5.8362 and U = 5.00.

(a)

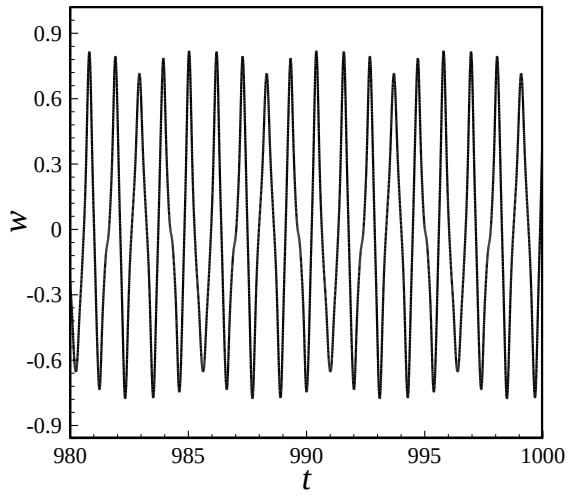

(b)

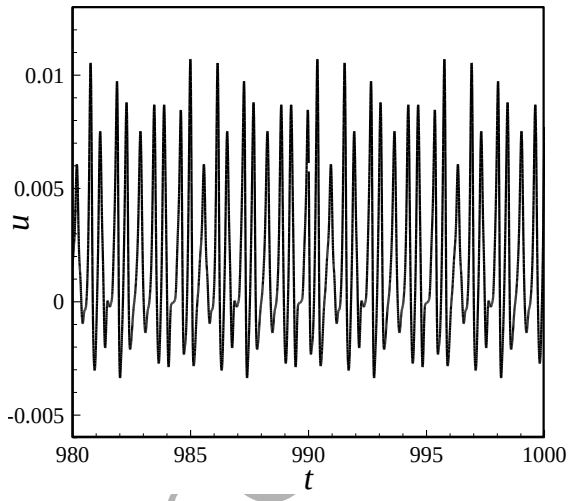

(c)

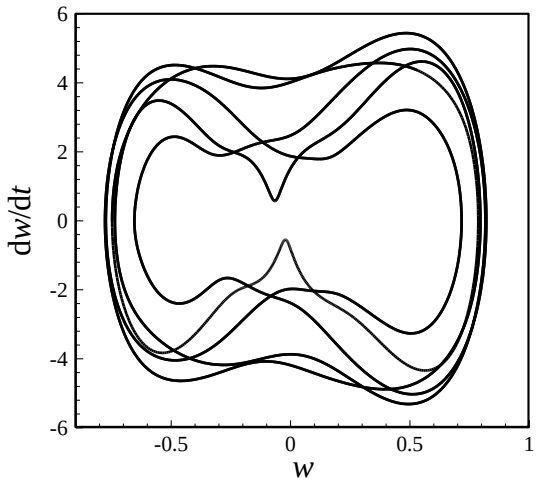

(d)

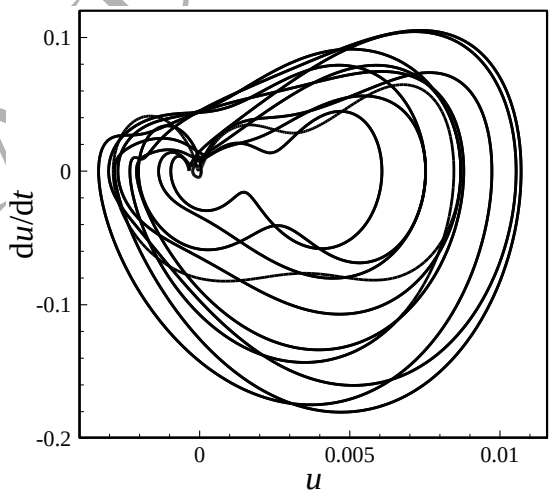

(e)

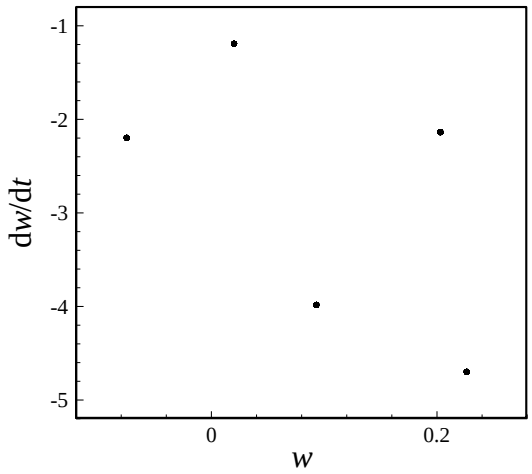

(f)

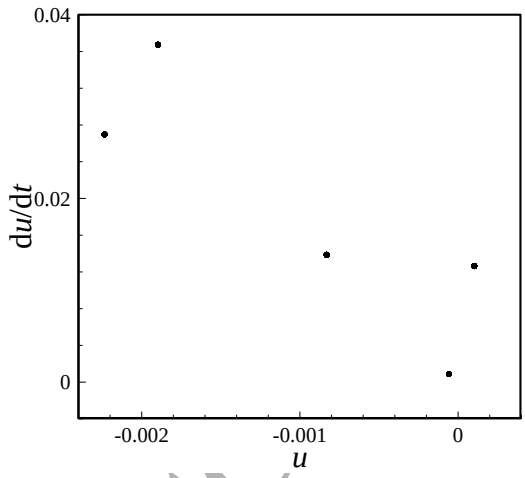

Figure 14: Motion characteristics at F_1=40.0 for the NSGT nanotube analysed in Fig. 11: (a) $w[x=0.5]$ against time; (b) $u[x=0.65]$ against time; phase-plane diagram for (c) $w[x=0.5]$ and (d) $u[x=0.65]$; Poincaré section for (e) $w[x=0.5]$ and (d) $u[x=0.65]$.

(a)

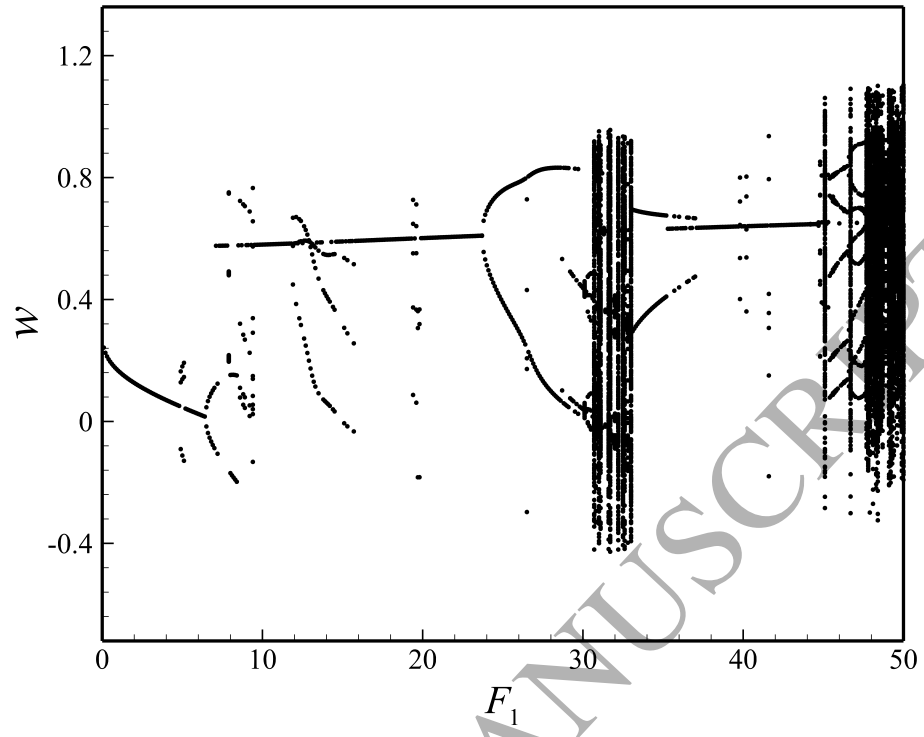

(b)

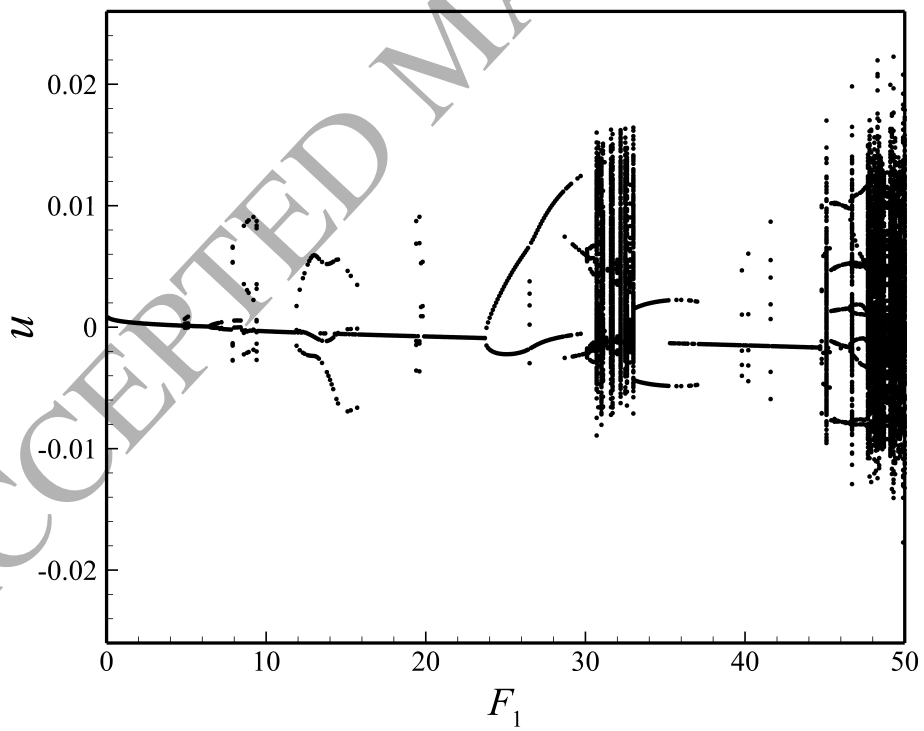

Figure 15: Bifurcation of fluid-conveying NSGT tubes: (a) motion in transverse axis (x=0.50); (b) motion in longitudinal axis (x=0.65); A_0=0.01, ω_1= 7.1186 and U = 5.00.

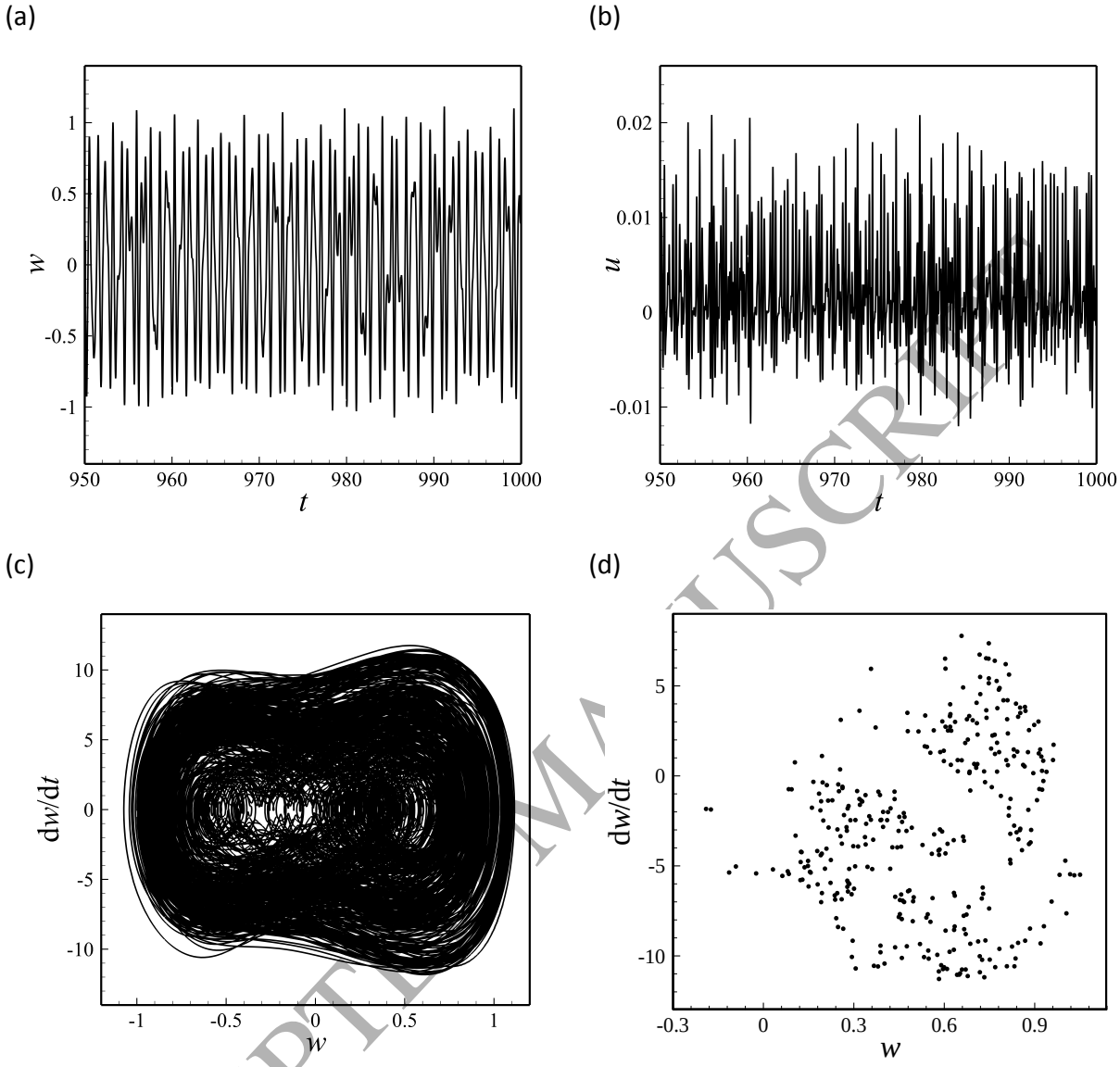

Figure 16: Motion characteristics at F_1=49.2 for the NSGT nanotube analysed in Fig. 13: (a) $w[x=0.5]$ against time; (b) $u[x=0.65]$ against time; (c) phase-plane diagram for $w[x=0.5]$; (d) Poincaré section for $w[x=0.5]$.

(a)

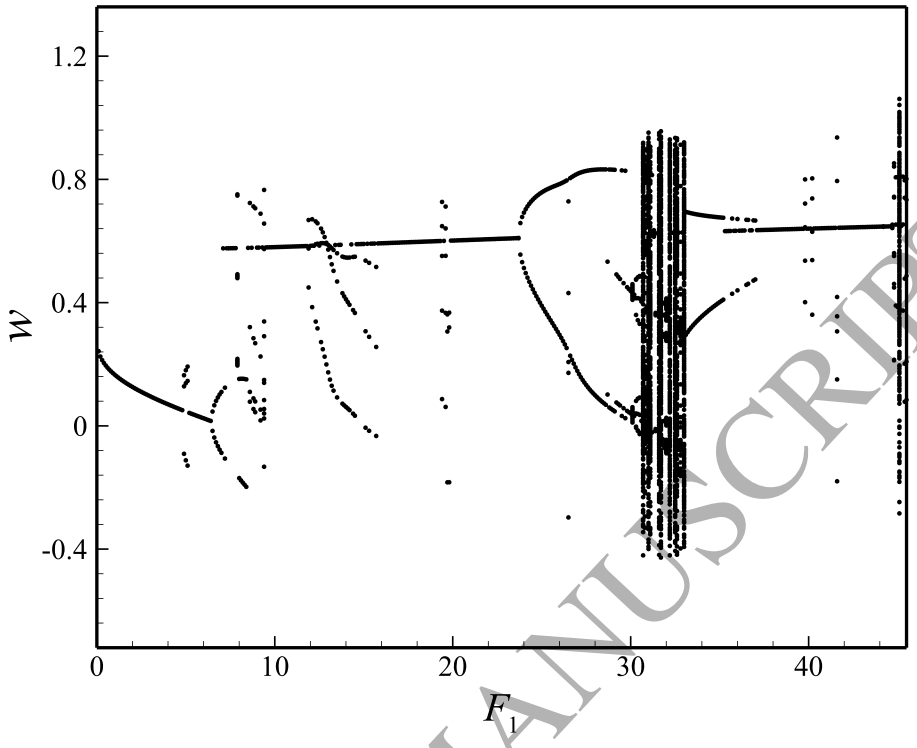

(b)

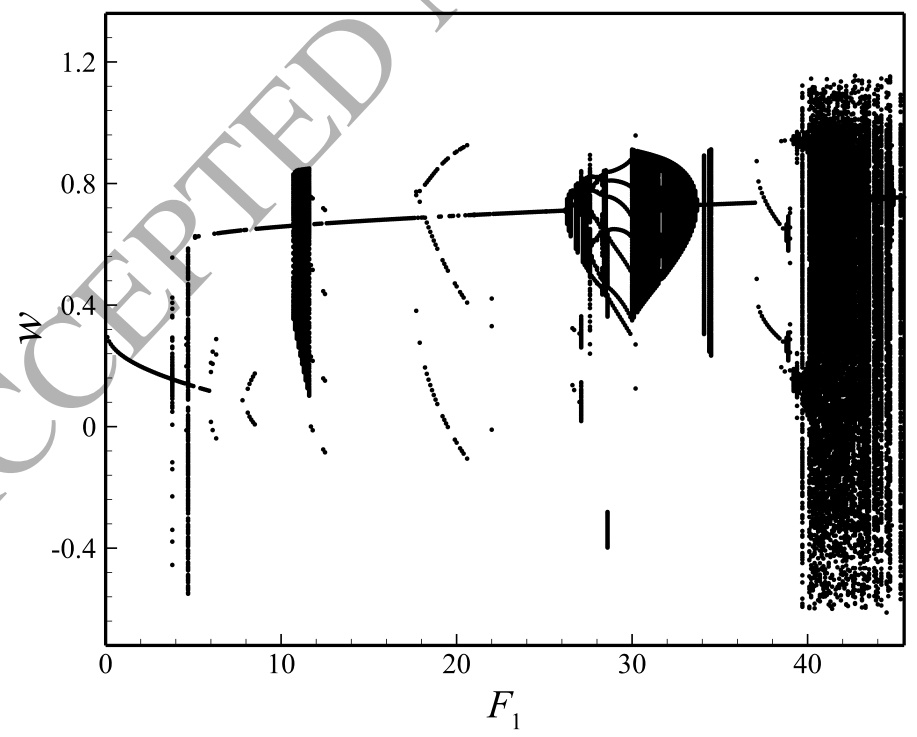

(c)

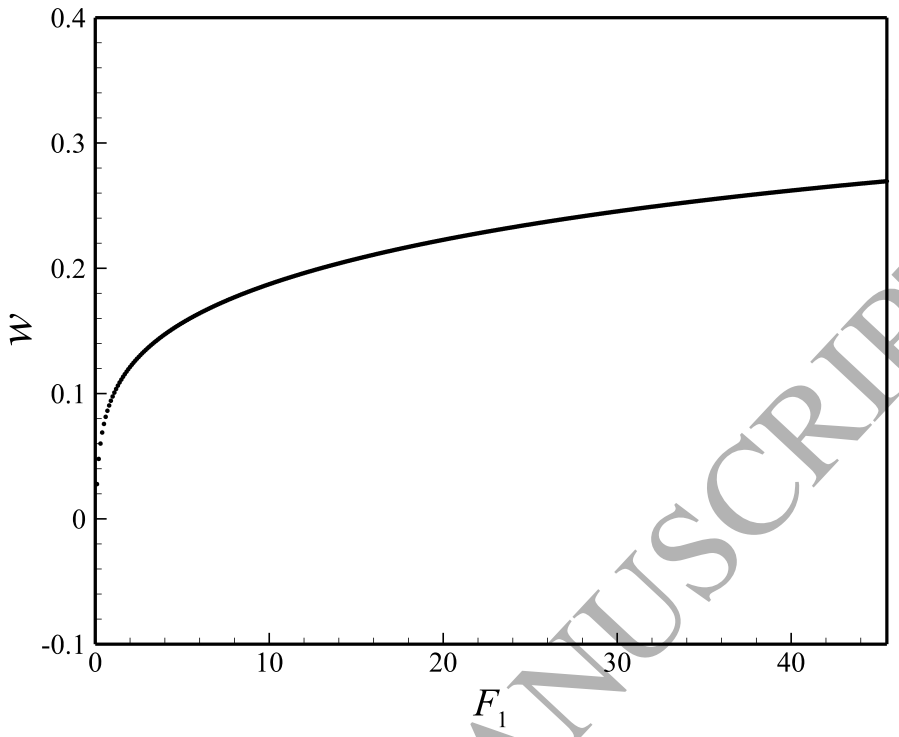

(d)

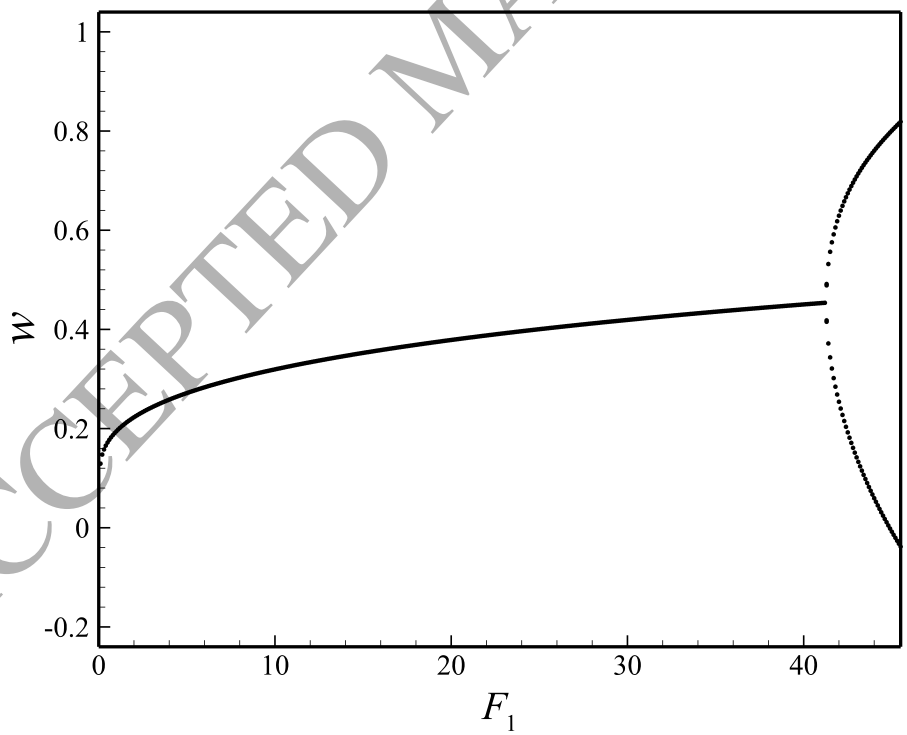

Figure 17: Size effects on bifurcation of fluid-conveying NSGT tubes for the transverse motion: (a) η_{sg} =0.04 and η_{nl} =0.10 (NSGT); (b) η_{sg} =0 and η_{nl} =0.10 (NET); (c) η_{sg} =0.04 and η_{nl} =0 (SGT); (d) η_{sg} =0 and η_{nl} =0 (CET).